CHEMICAL SYSTEMS LABORATORY CONTRACTOR REPORT

ARCSL-CR-82047

INVERSION TECHNIQUE EVALUATION

by

R. L. Henning
C. D. Capps
G. M. Hess

October 1982

Boeing Aerospace Company
P.O. Box 3999
Seattle, Washington 98124

Contract No. DAAK11-80-C-0109

US ARMY ARMAMENT RESEARCH AND DEVELOPMENT COMMAND
Chemical Systems Laboratory
Aberdeen Proving Ground, Maryland 21010

Disclaimer

The views, opinions, and/or findings contained in this report are those of the authors and should not be construed as an official department of the Army position, policy, or decision unless so designated by other documentation.

Disposition

Destroy this report when it is no longer needed. Do not return it to the originator.

UNCLASSIFIED

SECURITY CLASSIFICATION OF THIS PAGE *(When Data Entered)*

REPORT DOCUMENTATION PAGE

READ INSTRUCTIONS BEFORE COMPLETING FORM

1. REPORT NUMBER: ARCSL-CR-82047	2. GOVT ACCESSION NO.
3. RECIPIENT'S CATALOG NUMBER	
4. TITLE *(and Subtitle)*: INVERSION TECHNIQUE EVALUATION	5. TYPE OF REPORT & PERIOD COVERED: Final Report, Sept. 1980 to Feb. 1982
6. PERFORMING ORG. REPORT NUMBER	
7. AUTHOR(s): R. L. Henning, C. D. Capps, G. M. Hess	8. CONTRACT OR GRANT NUMBER(s): DAAK11-80-C-0109
9. PERFORMING ORGANIZATION NAME AND ADDRESS: Boeing Aerospace Company, P.O. Box 3999, Seattle, WA 98124	10. PROGRAM ELEMENT, PROJECT, TASK AREA & WORK UNIT NUMBERS
11. CONTROLLING OFFICE NAME AND ADDRESS: Commander, Chemical Systems Laboratory, Attn: DRDAR-CLJ-R, Aberdeen Proving Groun, MD 21010	12. REPORT DATE: October 1982
	13. NUMBER OF PAGES: 74
14. MONITORING AGENCY NAME & ADDRESS *(if different from Controlling Office)*: Commander, Chemical Systems Laboratory, Attn: DRDAR CLB-PS, Aberdeen Proving Ground, MD 21010	15. SECURITY CLASS. *(of this report)*: UNCLASSIFIED
	15a. DECLASSIFICATION/DOWNGRADING SCHEDULE: N/A

16. DISTRIBUTION STATEMENT *(of this Report)*

Approved for public release, distribution unlimited.

17. DISTRIBUTION STATEMENT *(of the abstract entered in Block 20, if different from Report)*

18. SUPPLEMENTARY NOTES

This study was sponsored by the US Army Smoke Research Program, Chemical Systems Laboratory, Aberdeen Proving Ground, MD. Contract Project Officer: Dr. Jerold Bottiger (DRDAR-CLB-PS, (301) 671-2326)

19. KEY WORDS *(Continue on reverse side if necessary and identify by block number)*

Optical inversion	Constrained linear inversion	Backus-Gilbert synthesis
Aerosols	Kernel covariance matrix	Landweber iteration
Elastic scattering	Military obscurants	Eigenanalysis
Homogeneous spheres	Direct inversion	Eigenfunctions
Mie theory	Principal components analysis	

20. ABSTRACT *(Continue on reverse side if necessary and identify by block number)*

An analytic method for inversion problems of the Fredholm integral type is developed. The application of this formalism to error analysis and optimal experimental design is discussed. Results from this method for simulated experimental data are compared with results from other commonly used inversion techniques.

DD FORM 1 JAN 73 1473 EDITION OF 1 NOV 65 IS OBSOLETE

UNCLASSIFIED

SECURITY CLASSIFICATION OF THIS PAGE *(When Data Entered)*

PREFACE

The work described in this report was performed by the Boeing Aerospace Company, Contract No. DAAK11-80-C-0109. The work covers the period 29 September 1980 to 1 February 1982.

The use of trade names in this report does not constitute an official endorsement or approval of the use of such commercial hardware or software. This report may not be cited for purposes of advertisement.

TABLE OF CONTENTS

		Page
1	INTRODUCTION	9
2	THE METHODS OF INVERSION	11
2.1	Direct Inversion	11
2.2	Constrained Linear Inversion	17
2.3	Landweber Iteration	18
2.4	Backus-Gilbert Synthesis	18
3	KERNEL OPTIMIZATION	19
3.1	Development of the Selection Scheme	20
3.1.1	Cluster Analysis	21
3.1.2	Eigenanalysis of the Covariance Matrix	21
3.2	The Optimization Technique	24
4	RESULTS	24
4.1	Optimization Results	25
4.1.1	Test Case Description	25
4.1.2	Test Case Results	26
4.1.3	Experimental Implications	28
4.2	Inversion results	29
4.2.1	Test Case Description	29
4.2.2	Test Case Results: Four Methods of Inversion	30
4.2.3	Direct Inversion Sensitivity Results	31
5	CONCLUSIONS AND RECOMMENDATIONS	34
	LITERATURE CITED	37
	BIBLIOGRAPHY	39
	APPENDICES	
	A. Tables	43
	B. Figures	45

LIST OF FIGURES

		Page
B-1	Direct Inversion Results for Three Materials.....	45
B-2	Direct Inversion Results: Sensitivity to Decreased Geometric Mean Diameter σ_g = 1.2, d_g = 1.2 Recoverable Fraction = 0.894.....	46
B-3	Direct Inversion Results: Sensitivity to Decreased Geometric Mean Diameter σ_g = 1.2, d_g = 1.0 Recoverable Fraction = 0.630.....	47
B-4	Direct Inversion Results: Sensitivity to Decreased Geometric Standard Deviation σ_g = 1.1, d_g = 1.6 Recoverable Fraction = 0.960.....	48
B-5	Direct Inversion Results: Sensitivity to Increased Geometric Standard Deviation σ_g = 1.4, d_g = 1.6 Recoverable Fraction = 0.984.....	49
B-6	Comparison of Results for the Four Inversion Methods: Noise Free.....	50
B-7	Comparison of Results for the Four Inversion Methods: 1% Noise.....	51
B-8	Comparison of Results for the Four Inversion Methods: 10% Noise.....	52
B-9	Direct Inversion Results for Three Noise Levels.....	53
B-10	Direct Inversion Results for Varying Number of Measurements.	54
B-11	The Ten Most Significant Eigenfunctions for the Baseline Case: ϕ1.....	55
B-12	The Ten Most Significant Eigenfunctions for the Baseline Case: ϕ2.....	56
B-13	The Ten Most Significatn Eigenfunctions for the Baseline Case: ϕ3.....	57
B-14	The Ten Most Significant Eigenfunctions for the Baseline Case: ϕ4.....	58
B-15	The Ten Most Significant Eigenfunctions for the Base Case: ϕ5.....	59

List of Figures (Continued)

		Page
B-16	The Ten Most Significant Eigenfunctions for the Baseline Case: $\phi 6$	60
B-17	The Ten Most Significant Eigenfunctions for the Baseline Case: $\phi 7$	61
B-18	The Ten Most Significant Eigenfunctions for the Baseline Case: $\phi 8$	62
B-19	The Ten Most Significant Eigenfunctions for the Baseline Case: $\phi 9$	63
B-20	The Ten Most Significant Eigenfunctions for the Baseline Case: $\phi 10$	64
B-21	Direct Inversion Sensitivity to Extended Radius Range: Baseline Twelve Measurements	65
B-22	Direct Inversion Sensitivity to Extended Range and Distribution: Bimodal	67
B-23	Direct Inversion Sensitivity to Extended Range and Distribution: Increased Geometric Mean Diameter	68

INVERSION TECHNIQUE EVALUATION

1. INTRODUCTION

Aerosol particle size distributions are currently determined using discrete sampling techniques such as aerodynamic or single particle optical classification. These methods, although straightforward in application, have practical limitations. The statistical nature of the sampling process has the inherent limitation of sample size; a sufficient number of measurements must be made to insure meaningful results. The measurements are also labor intensive. These considerations translate directly into the cost of determining the size distribution.

A technique that incorporates integral rather than discrete measurements has the potential to provide a rapid and less costly determination of the particle size distribution. Such a technique requires analytic inversion of the integral relationship between the measurements and the particle size distribution. The purpose of this study is to determine the applicability of the inversion process to laboratory and field measurements for spherical, homogeneous, single scattering particles of known complex index of refraction. Analytic kernels for scattering and extinction by this limited class of particles are found using Mie theory. The Mie kernels are used in conjunction with a particle size distribution to express intensity measurements in the Fredholm integral equation

$$\mathbf{g}(\lambda, \theta, \rho) = \int_a^b \mathbf{K}(\alpha, \theta, n, k, \rho)\ f(r)\ dr + \epsilon_i \qquad (1)$$

where

$\mathbf{g}$ = intensity measurements
λ = incident wavelength
θ = scattering angle
ρ = polarization
$\mathbf{K}(\alpha, \theta, n, k, \rho)$ = Mie kernels
α = size parameter $2\pi r/\lambda$
$n-ik$ = complex index of refraction

f = particle size distribution

r = particle radius

ε_i = experimental error

Several methods of inversion, including constrained linear inversion, Backus-Gilbert synthesis, Landweber iteration, and direct inversion, are to be compared using quantitative figures of merit and qualitative assessment of the effects of constraints inherent to each method.

It would be desirable to know, when designing an experiment, which measurements would provide the most information about a particular class of aerosols. Considering that several wavelength-angle-polarization combinations could be used to measure the scattering or extinction by an aerosol sample, linearly independent kernels would clearly be preferred; that is, the values of the kernels as a function of particle radius should not be just multiples or sums of each other. This report discusses each of the inversion methods, details an optimization scheme for selecting independent kernels from a set of candidate kernels, and gives a comparative evaluation of inversion results for optimized kernel subsets.

At the same time that this study was being conducted for the US Army, the direct method of inversion was developed independently by Boeing from the work of Twomey[1] for the purpose of gaining physical insight into both the kernel selection and inversion portions of problems of this type. We found that the direct method not only treats error effects in a straightforward manner, but also provides key insights into the physical limitations set by the kernels of the measurements to be inverted. Direct inversion provides validation of the kernel optimization technique by giving a quantitative measure of recoverable information from a kernel set for a given expected particle size distribution. Useful inversion results are obtained by direct inversion for the test cases studied at experimental noise levels of one and ten percent. For the test cases studied, direct inversion results are superior to constrained linear inversion and Backus-Gilbert results. Landweber iteration performs as well as direct inversion, but adds no understanding of how well a given set of measurements and kernels is expected to perform on inversion. Using the concept of the recoverable information fraction, we see that no method

of inversion will give more information about the actual distribution without adding information through smoothing constraints.

One could argue that knowledge of certain physical processes, such as drop formation, implies a particle size distribution with a given form, and therefore a trial solution with that form could be used as a meaningful smoothing constraint. However, given this type of explicit knowledge, improved results could probably be obtained by using parameter fitting to the curve type instead of inverting noisy data. Other smoothing techniques, such as minimizing a particular order derivative of the returned funtion, obscure physical interpretation of the inversion process and offer no clearly justifiable method for deciding how much smoothing should be used.

2. THE METHODS OF INVERSION

The purpose of inversion is to extract the desired solution f from the family of solutions that satisfy equation 1. Truly analytic inversion requires error free measurements and continuous knowledge of the kernels over a large interval. A useful inversion technique must use numerical approximations of this continuous knowledge, and must provide for ascertaining the stability of a solution in the presence of experimental noise.

2.1 Direct Inversion

Several years ago S. Twomey[1] published a technique for determining the "information content" in a set of remote sensing measurements. This section will show how Twomey's method, with some modification, can be used as the basis for analytic inversion of indirect sensing experiments. In addition, this modified method gives the quantitative information that enables the experimentalist to select the optimal measurements, from a set of possible measurements, that will provide the desired information. Throughout this work, the notation of reference 1 will be used wherever possible to facilitate comparison. In order to derive the inversion formula, the error ϵ_i will be ignored until an expression has been obtained. The effects of error may then be calculated.

Let V be the vector space over the reals consisting of all continuous, real-valued functions on the closed interval (a, b), and the inner product on V be

$$< t, u> = \int_a^b t(x)\ u(x)\ dx \qquad t, u \in V \qquad (2)$$

The norm $||\ u\ ||$ of a function u(x) is then

$$||\ u\ || = < u, u>^{1/2} \qquad (3)$$

Throughout this section it will be assumed that equation 1 has been normalized such that

$$||\ K_i\ || = 1 \qquad i = 1, 2, \ldots, N \qquad (4)$$

If W is the subspace of V spanned by the $K_i(x)$ and X is the orthogonal complement of W in V, then the function f(x) can be written

$$f(x) = r(x) + s(x) \qquad r(x) \in W,\ s(x) \in X \qquad (5)$$

assuming that f(x) is a continuous, real-valued function.

This expression differs from equation 2 of Twomey in that the latter expression is equivalent to the assumption that f(x) lies entirely in W, an assumption which is not generally true. It follows from the definition of the orthogonal complement that

$$g_i = \int_a^b K_i(x)\ f(x)\ dx = \int_a^b K_i(x)\ \{r(x) + s(x)\}\ dx$$

$$= \int_a^b K_i(x)\ r(x)\ dx \qquad (6)$$

This implies that only r(x), the portion of f(x) lying in the space spanned by the kernels $K_i(x)$, will have experimental consequences and, hence, be obtainable by inversion of the measurements. This ambiguity is inherent in any inversion technique and shows the importance of carefully choosing the $K_i(x)$ to maximize retrievable information.

An orthonormal basis for W can be constructed from an eigenanalysis of the covariance matrix **C**, where the element in the ith row and jth column of C is given by

$$c_{ij} = \langle K_i, K_j \rangle \tag{7}$$

As **C** is a real, symmetric matrix, its eigenvalues are real and non-negative. Let $\mathbf{\Lambda}$ be the diagonal matrix that contains the eigenvalues of **C** in descending order, and

let **U** be the eigenvector matrix containing the corresponding unit normalized eigenvectors of the covariance matrix in its columns. Let the square root of a diagonal matrix be given by the diagonal matrix with elements equal to the square roots of the respective elements of the original matrix. If **K**(x) is the column matrix whose elements are the functions $K_i(x)$, and the asterisk denotes matrix transposition, an orthonormal basis $_i(x)$ for W is given by

$$\boldsymbol{\phi}(x) = \mathbf{\Lambda}^{-1/2}\, \mathbf{U}^*\, \mathbf{K}(x) \tag{8}$$

The proof that the $\phi_i(x)$ are orthonormal is given by Twomey. The function r(x) is an element of W and the $\phi_i(x)$ form an orthonormal basis of W. Therefore, r(x) can be expressed as a linear combination of the $\phi_i(x)$ as follows:

$$r(x) = \boldsymbol{\xi}^*\, \boldsymbol{\phi}(x) = \boldsymbol{\phi}^*(x)\, \boldsymbol{\xi} \tag{9}$$

where the ξ_i are the coefficients of the basis vectors of W.

Expressing equation 6 in matrix form,

$$\mathbf{g} = \int_a^b \mathbf{K}(x)\, r(x)\, dx$$

$$= \int_a^b \mathbf{K}(x)\, \boldsymbol{\phi}^*(x)\, \boldsymbol{\xi}\, dx$$

$$= \int_a^b \mathbf{K}(x)\, \mathbf{K}^*(x)\, dx \;\; \mathbf{U}\, \mathbf{\Lambda}^{-1/2}\, \boldsymbol{\xi}$$

$$= \mathbf{C}\,\mathbf{U}\,\mathbf{\Lambda}^{-\frac{1}{2}}\,\xi$$

$$= \mathbf{U}\,\mathbf{\Lambda}^{\frac{1}{2}}\,\xi \qquad (10)$$

Since the eigenvectors are orthonormal the above equation may easily be solved for the coefficients of the ϕ_i.

$$\xi = \mathbf{\Lambda}^{-\frac{1}{2}}\,\mathbf{U}^*\,\mathbf{g} \qquad (11)$$

This gives the analytic solution to the inversion problem.

$$r(x) = \mathbf{K}^*(x)\,\mathbf{U}\,\mathbf{\Lambda}^{-1}\,\mathbf{U}^*\,\mathbf{g} \qquad (12)$$

Equation 12 is formally equivalent to Twomey's equation 5; however, the interpretation of the left-hand side is different. This may be seen by taking a known f(x), calculating the g_i's, and using these values in the inversion process. Twomey's equation 5 implies that f(x) should be obtained exactly. From the preceeding analysis, only r(x), that portion of f(x) lying in the space spanned by the kernels, can be recovered. A convenient measure is obtained by comparing the norms of r(x) and f(x).

$$||\ r\ ||^2 = \int_a^b \{r(x)\}^2\ dx$$

$$= \int_a^b \xi^*\,\phi(x)\,\phi^*(x)\,\xi\ dx$$

$$= \xi^*\,\mathbf{I}\,\xi$$

$$= \xi^*\,\xi \qquad (13)$$

where $\mathbf{I}$ is the identity matrix of appropriate order. The norm of f(x) is given by

$$||\ f\ ||^2 = \int_a^b \{f(x)\}^2\ dx$$

$$= \int_a^b \{r(x) + s(x)\}^2\ dx$$

$$= \int_a^b \{\xi^* \phi(x) + s(x)\}^2 \, dx$$

$$= \xi^* \xi + 2\xi^* \Lambda^{-1/2} U \int_a^b K(x)\, s(x)\, dx + \int_a^b \{s(x)\}^2 \, dx$$

$$= \xi^* \xi + || s ||^2 \qquad (14)$$

Comparing equation 13 and equation 14, the norm of r(x) must always be less than or equal to the norm of f(x).

$$\frac{|| r ||}{|| f ||} \leq 1 \qquad (15)$$

Returning now to the original problem of an unknown f(x) and errors in the experimental g_i's, we can calculate the effect of these errors on the inverted function r(x). Rewriting equation 12 in a different form yields

$$r(x) = \phi^*(x) \Lambda^{-1/2} U^* g$$

$$= \Sigma \alpha_i g_i \qquad (16)$$

where

$$\alpha_i = \sum_j \frac{\phi_j(x)}{\sqrt{\lambda_j}} u_{ij}$$

If the ϵ_i of equation 1 are the standard deviations of the normally distributed, zero-mean error in the g_i's, then the variance $\{\delta(x)\}^2$ of r(x) is

$$\{\delta(x)\}^2 = \sum_i \alpha_i^2 \epsilon_i^2 \qquad (17)$$

The norm of $\delta(x)$ is then

$$|| \delta ||^2 = \int_a^b \{\delta(x)\}^2 \, dx$$

$$= \sum_{ijk} \frac{u_{ij}}{\sqrt{\lambda_j}} \frac{u_{ik}}{\sqrt{\lambda_k}} \epsilon_i^2 \int_a^b \phi_j(x)\, \phi_k(x)\, dx$$

$$= \sum_{ijk} \frac{u_{ij}}{\sqrt{\lambda_j}} \frac{u_{ik}}{\sqrt{\lambda_k}} \epsilon_i^2 \delta_{jk}$$

$$= \sum_j \lambda_j^{-1} \sum_i u_{ij} \epsilon_i^2 \qquad (18)$$

A simple expression for an upper bound on equation 15 may be obtained using the unit normal property of the eigenvectors.

$$|| \delta ||^2 = \sum_j \lambda_j^{-1} \sum_i u_{ij}^2 \epsilon_i^2$$

$$\leq \sum_j \lambda_j^{-1} \{\sum_i u_{ij}^2\} \{\sum_i \epsilon_i^2\}$$

$$\leq |\epsilon|^2 \sum_j \lambda_j^{-1} \qquad (19)$$

where the vector $\boldsymbol{\epsilon}$ is the column matrix containing the standard deviations ϵ_i, and $|\ |$ denotes the magnitude of a vector. A similar expression for $||\ r\ ||$ may be derived using the fact that the λ_i's are non-negative.

$$|\mathbf{g}|^2 = \mathbf{g}^* \mathbf{g}$$

$$= \boldsymbol{\xi}^* \boldsymbol{\Lambda}^{1/2} \mathbf{U}^* \mathbf{U} \boldsymbol{\Lambda}^{1/2} \boldsymbol{\xi}$$

$$= \boldsymbol{\xi}^* \boldsymbol{\Lambda} \boldsymbol{\xi}$$

$$= \sum_i \lambda_i \xi_i^2$$

$$\leq \{ \sum_i \lambda_i \} \{ \sum_i \xi_i^2 \}$$

$$\leq \{ \sum_i \lambda_i \} \boldsymbol{\xi}^* \boldsymbol{\xi}$$

$$\leq \{ \sum_i \lambda_i \} ||\ r\ ||^2 \qquad (20)$$

Equations 19 and 20 lead to an upper bound on the ratio of the norms of the standard deviation in r(x) to the norm of r(x), referred to as the relative error in r(x), in terms of the relative error in g, where the relative error in g is given by the ratio of the magnitude of the standard deviation vector to the magnitude of g.

$$\frac{||\ \delta\ ||}{||\ r\ ||} \leq \{\ \sum_i \lambda_i^{-1}\}^{1/2}\ \{\ \sum_i \lambda_i\}^{1/2}\ \frac{|\epsilon|}{|g|} \qquad (21)$$

Given a relative error in **g** the relative error in r(x) is controlled by the factor involving λ_i^{-1}. Since the λ_i's are arranged in decreasing order, the more eigenvalues that are kept for the analysis, the larger the error in the returned function becomes. Thus, for a desired uncertainty in the returned function r(x) only $p \leq N$ eigenvalues and eigenvectors can be used in equation 12. The consequence of this is that only p orthogonal functions can be used to expand r(x). Comparing our analysis with Twomey's shows that his "pieces of information" are the number of independent functions, lying in the space spanned by the p eigenfunctions (given by equation 8), into which f(x) can be reliably decomposed.

2.2 Constrained Linear Inversion.

Constrained linear inversion begins with the quadrature approximation to equation 1 given by

$$\mathbf{g} = \mathbf{A}\ \mathbf{f} \qquad (22)$$

where

g = measurement vector
A = kernel quadrature matrix
f = vector of actual distribution

The approach is to minimize some arbitrary nonnegative smoothing measure of the inverted solution **f'**, while holding constant the error $\boldsymbol{\epsilon}$ in the expression

$$\mathbf{A}\ \mathbf{f}' - \mathbf{g} = \boldsymbol{\epsilon} \qquad (23)$$

Some commonly used smoothing properties include minimum departure from a trial function and minimization of a particular order derivative of the inverted function. Using the method of Lagrange multipliers to solve this constrained minimization problem, we have

$$\frac{\delta}{\delta f'} \{ (A f' - g)^* (A f' - g) + \gamma (f'^* H f') \} = 0 \qquad (24)$$

where **H** is the derivative smoothing matrix. Simplification of equation 24 yields

$$f' = (A^* A + \gamma H)^{-1} A^* g \qquad (25)$$

The smoothing parameter γ can be interpreted as a filter that eliminates small eigenvalues from the kernel covariance matrix. In practice, the magnitude of γ is determined by starting with a low value and increasing γ until the sum squared residual of

$$A f' - g \qquad (26)$$

is approximately equal to the expected measurement errors in the g data. Further discussion of the constrained linear inversion technique may be found in references 1 and 2.

2.3 Landweber Iteration.

The Landweber iterative approach succesively alters an initial estimate of the solution until sufficient convergence occurs. The solution corresponding to j iterations, f_j, is given by

$$f_j = f_{j-1} + (A^* A + \beta I)^{-1} A^* (g - A f_{j-1}) \qquad (27)$$

The smoothing parameter β must be chosen to compromise between large deviations from the trial distribution f_{j-1} and large residual components of **Af-g.** By equation 25, the first iteration of Landweber is equivalent to constrained linear inversion. Details on the development of Landweber iteration and proofs of convergence properties are available in references 3 and 4.

2.4 Backus-Gilbert Synthesis.

The main concept used in Backus-Gilbert synthesis is the construction of linear combinations of kernels that approximate Dirac delta functions at the radii of interest. There are two major opposing concerns that must meet a compromise

for successful Backus-Gilbert synthesis: (1) the effect of error in the measurements on the solution, or variance; and (2) the mean square difference of the synthesized functions and Dirac delta functions, or resolution. The principal equations used are given by

$$\mathbf{a}(\theta) = (\mathbf{u}^* \, W(\theta) \, \mathbf{u})^{-1} \, W(\theta)^{-1} \, \mathbf{u} \qquad (28)$$

where

$$u_i = \int_a^b K_i(r) \, dr$$

$W(\theta) = \mathbf{S} \cos\theta + c \, \mathbf{S}_\epsilon \sin\theta$

$\mathbf{S}$ = resolution matrix

$\mathbf{S}_\epsilon$ = variance matrix

θ = tradeoff parameter

c = arbitrary constant

$\mathbf{a}(\theta)$ = coefficient vector of linear combination of kernels

Further discussion of Backus-Gilbert synthesis is found in references 5 and 6.

3. KERNEL OPTIMIZATION

Selection of the absolute optimal subset, with respect to information content, from a large set of candidate measurements would require evaluation of each possible combination of the desired number of measurements. If p measurements were to be selected from q candidates, the number of subsets to examine is given by

$$\binom{q}{p} = \frac{q!}{p!(q-p)!} \qquad (29)$$

Selecting even just a few measurements from a larger set rapidly requires comparison of an unmanageable number of subsets. For practical purposes, an approximate method for optimization is needed, together with a measure of how close the subset comes to including all of the information available in the full set of measurements. Section 3.1 highlights the advantages and shortcomings of several optimization schemes that were investigated. The present optimization algorithm,

described in section 3.2, retains many of the advantages and minimizes the shortcomings of the investigated optimization schemes.

3.1 Development of the Selection Scheme.

The dependencies between kernels, and hence measurements, are reflected by the kernel covariance matrix. A perfectly uncorrelated set of normalized kernels would produce a covariance matrix with ones on the diagonal and zeros everywhere else. Mie kernels corresponding to experimentally feasible measurements are typically quite correlated, and require eigenanalysis to untangle the dependencies and identify how many pieces of information are truly available in the kernel set.

Principal components analysis forms factors, or linear combinations of the kernels, such that the coefficient vectors defining each factor are orthogonal and have unit length. The factors are extracted so that each successive factor maximizes the remaining variance. The mathematical equation for extracting the ith factor is given by

$$\frac{\delta}{\delta \mathbf{q}_i} \{ (\mathbf{q}_i^* \mathbf{C} \mathbf{q}_i) + \eta (1 - \mathbf{q}_i^* \mathbf{q}_i) \} = 0 \qquad (30)$$

where

$\mathbf{q}_i$ = coefficient vector of ith linear combination

$\mathbf{C}$ = covariance matrix with eigenvalues 1 to i-1 deleted

η = Lagrange multiplier

Simplifying equation 30 yields the result that the coefficient vector for the ith factor is the eigenvector of the kernel covariance matrix corresponding to the ith largest eigenvalue, λ_i. The amount of variance contributed by the ith factor is

$$\frac{\lambda_i}{tr(\mathbf{K}^* \mathbf{K})} \qquad (31)$$

where $tr(\mathbf{K}\mathbf{K}^*)$ = trace$(\mathbf{K}\mathbf{K}^*)$ = sum of diagonal elements of $\mathbf{K}\mathbf{K}^*$.

3.1.1 Cluster Analysis.

Most of the variance in the system is contained in just a few factors when dealing with dependent kernels, so the dimensionality of the system may be reduced by retaining only as many factors as needed to acccount for most of the variance. The result of projecting the kernels onto this smaller, orthogonal set of axes defined by the factors is a representation of the kernels as points in p-space, where p is the number of contributing factors. The kernels can then be compared and clustered into similarity groups on the basis of simple distance.

Clustering results give the distance levels at which each kernel joins a growing cluster. The number of clusters present at some given distance gives an intuitive idea of the information content of the kernel set. However, the non-physically interpretable step of projecting the kernels onto the orthogonal factors introduces difficulties into the determination of a rigorous distance level criterion for establishing the number of clusters. There is also no guarantee that the most independent subset of kernels would necessarily be far apart in the factor space. The principal components portion of the analysis does, however, provide a tool for constructing a set of orthogonal functions that have the same dimensionality as the kernels.

3.1.2 Eigenanalysis of the Covariance Matrix.

For the cluster analysis optimization scheme, principal components analysis was used as a preprocessor of the kernel functions in order to produce variables upon which synthetic kernels could be defined by projection of the old kernels onto the new variables. The eigenfunctions of the covariance matrix were, in this case, linear combinations of the radius variables. This form of principal components analysis, without the cluster analysis, would identify which radius measurements would be appropriate for a given set of wavelength-angle-polarization combinations. It would be more desirable to identify which wavelength-angle-polarization measurements would be suitable for a given range of radii.

An element of the kernel covariance matrix that corresponds to wavelength identification, for example, for a radius range from a to b is given by

$$\int_a^b K_i(r)\, K_j^*(r)\, dr \qquad (32)$$

where

r = particle radius

K_i = Mie kernel for $\mathbf{K}(\lambda_i, r)$

λ_i = incident wavelength of ith measurement

In matrix notation, the kernel covariance matrix is given by

$$\mathbf{K}\,\mathbf{K}^* \qquad (33)$$

where

$\mathbf{K}$ = mxn kernel matrix

m = number of measurements

n = number of radii

$k_{ij} = \mathbf{K}(\lambda_i, r_j)$

whereas the covariance matrix used for cluster analysis preprocessing is given by

$$\mathbf{K}^*\,\mathbf{K} \qquad (34)$$

The eigenvectors of the kernel covariance matrix are linear combinations of the wavelength kernels that are orthogonal and of length unity. To identify the most important kernels from these linearly independent combinations, consider the matrix $\mathbf{U}$ containing the eigenvectors of the kernel covariance matrix such that the ith column of the matrix is the ith eigenvector. The elements of largest magnitude identify the major contributing kernels to particular kernel combinations. However, there is no accounting for the exclusion of kernels that describe highly oscillatory components of the desired function that are perhaps irretrievable due to measurement error. That is, a particular kernel may account for most of the structure of one particular combination, but that combination may in turn contribute only a minute portion of the total variance. Variations of this maximum element selection criterion included: (1) selecting the maximum element from the eigenvector matrix, where each column was additionally weighted by a power of its corresponding eigenvalue; and (2) selecting the kernels with maximum variance as given by the largest contributions overall to significant eigenvectors,indicated by the maximum sums of the squares of the rows of the eigenvalue weighted eigenvector matrix. The groups resulting from these different selection techniques were similar, but examples were easily found for which the selection techniques would choose clearly non-optimal subsets. For example, the selection by maximum

variance method would choose two very nearly parallel kernels if they were both orthogonal to the remaining kernels.

Yet another method of selection utilizing eigenanalysis of the kernel covariance matrix is to maximize the amount of recoverable information from a set of kernels. From section 2.1, we have seen that the desired distribution f(x) is composed of functions orthogonal to the kernels as well as functions in the space spanned by the kernel set

$$f(x) = r(x) + s(x) \tag{35}$$

where r(x) is the recoverable function, or the function in the space spanned by the kernels, and s(x) is the portion of the function that lies outside the kernel space. By selecting kernels such that $||\ r(x)\ ||/||\ f(x)||$ is maximized, the maximum amount of recoverable information about f(x) is retained. Assume, for the moment, an analytic f(x) similar to the expected experimental distribution. Using the g_i from

$$g_i = \int_a^b K_i(x)\ f(x)\ dx \tag{36}$$

we have

$$r(x) = \xi^*\ \Lambda^{-\frac{1}{2}}\ U^*\ K(x) \tag{37}$$

and

$$\xi = \Lambda^{-\frac{1}{2}}\ U^*\ g \tag{38}$$

The measure of the fraction of information retrievable is given by

$$\frac{||\ r\ ||}{||\ f\ ||} = \left\{ \frac{\xi^*\ \xi}{\int f^2(x)} \right\}^{\frac{1}{2}} \tag{39}$$

and is a useful measure for comparing kernel groups selected by any optimization scheme. Explicit information about the dependencies among the kernels is ultimately given by the kernel covariance matrix itself. The concepts to develop

are then analysis of the kernel covariance matrix, and the fraction of recoverable information.

3.2 The Optimization Technique.

The kernel covariance matrix has elements c_{ij} defined by

$$c_{ij} = \int_a^b K_i(r)\, K_j^*(r)\, dr \qquad (40)$$

The kernels have been normalized such that $c_{ij} = 1$ when i=j. The first inclination one might have is to select the two kernels that have the smallest covariance, and then add on more kernels using a similar criterion. The problem with this reasoning is that the optimal subset of, say, five members does not necessarily contain the optimal four-subset. The number of possibilities becomes overwhelming.

In order to approximate the solution of this enumeration problem, assume that a finite set of kernels is given to choose from. The optimization technique we found to be most satisfactory iterates through an elimination procedure that identifies and deletes the most dependent kernel of each successively smaller subgroup. The specific procedure is to: (1) Sort through the kernel covariance matrix for the largest off diagonal element, c_{ij}. (2) Calculate SS_i, the overall correlation of kernel i with the others, given by the sum of the squares of the ith row elements. (3) Calculate SS_j, the sum of the squares of the jth column elements. (4) Delete the row and column i (eliminate measurement i) if SS_i if larger than SS_j, otherwise delete row and column j (eliminate measurement j). (5) The index of the deleted row and column indicates the most dependent kernel. Return to step 1 and continue until only p kernels remain. There is no guarantee that this method indeed selects the optimal kernel subset. This method has, however, produced superior results for the fraction of recoverable information as well as for actual inverted distributions for noise-free and noisy measurements.

4. RESULTS

Scattering kernels were generated using J.V. Dave's routine[7] for computing Mie functions. The kernels were used for generating the quadrature weighted kernel

matrices, kernel covariance matrices, and synthetic measurement data. The number of points used to approximate the integral equation 1 was set at 500 in order to compromise between computing time and necessary accuracy. Initially confounding poor results from good kernel sets pointed out the need to evaluate the kernels at precisely the same radii for kernel matrix, covariance matrix, and synthetic measurement calculations. This requirement indicates that finer resolution for numerical integration is needed, even though the values of the approximated integrals showed variations of only fractions of a percent as several hundred integration points within the fixed interval were added. Overall, we expected an error level of approximately 0.1% to accrue throughout the various numerical calculations executed in the course of generation and eigenanalysis of the kernel covariance matrix with the functions evaluated at 500 points.

Normalization was found to be of critical importance as the investigation proceeded. Without normalization, kernels that described different portions of the radius range in a structurally nonoverlapping manner could easily appear to be totally dependent as the effect of magnitude was overemphasized. To circumvent the magnitude problem, the kernels were normalized such that

$$\int_a^b K_i(r)\, K_i^*(r)\, dr = 1 \qquad (41)$$

where $K_i(r)$ is $\mathbf{K}(\lambda_i,r)$. These normalized kernels were then used to generate synthetic intensity data and the kernel covariance matrix.

4.1 Optimization Results.

4.1.1 Test Case Description.

The baseline set of kernels optimized consisted of unpolarized direct backscatter kernels for 85% by weight phosphoric acid smoke at forty wavelengths evenly spaced between 0.2660 and 10.3000 microns. The range of radii considered extended from 0.001 to 1.3 microns. For a given particle size distribution, the amount of recoverable information from a set of kernels may be calculated by equation 39. The particle size distribution used for this purpose, as well as for

generating the synthetic data, was a lognormal distribution with geometric mean diameter of 1.6 and geometric standard deviation of 1.2. The baseline kernel set was then compared to several other kernel sets.

The alternative sets included kernels that were: (1) identical to the baseline in all parameters except the sample material was water fog; (2) identical in all parameters except the sample material was fog oil; (3) identical in all parameters except the angular resolution was increased to $\pm 1^{\circ}$; (4) for 40 scattering angles between 0° and 40° and an incident wavelength of 1.06 microns; (5) for forty scattering angles between 0° and 20° and incident wavelength of 0.2660 micron; (6) for incident wavelength of 10.300 microns and 20 angles between 0° and 180° for parallel and perpendicular polarizations separately; (7) for incident wavelength of 0.2660 microns and 20 angles between 0° and 180° for each of the polarizations.

4.1.2 Test Case Results.

A summary of results for the baseline and the seven additional cases is given in Table 1. The baseline case and the first two variations show that there is only a minute component of the particle size distribution that is orthogonal to each kernel set for the three materials under consideration. The third case results are very similar to the baseline case results, indicating that experimentally achievable angular resolutions will not degrade the information content of discrete angle kernels. Kernel sets with angular variation for a fixed wavelength show a noticeable drop in the fraction of recoverable information in cases four and five, and indicate that for unpolarized kernels, wavelength variation is preferable to angular scanning. Separating the polarizations does nothing to improve the information content of angular scan data, as illustrated by cases six and seven. Comparing cases four and six with cases five and seven indicates that the shorter wavelengths produce kernels with more recoverable information if angular scanning data is to be used. At times, the error level exceeds the expected 0.1% error, giving a recoverable fraction value greater than one. For these cases, the number of significant eigenvectors is equal to the maximum number of eigenvectors for which the recoverable fraction is less than one.

Table 1. Information Content in Variations of the Baseline Case

Case	Significant Eigenvectors	Fraction of Recoverable Information
BASELINE: H_3PO_4 40 wavelengths 0.266-10.3 microns 0.001-1.3 micron radius Backscatter kernels Lognormal distribution with σ_g=1.2, d_g=1.6	14	0.997
1. Water fog	14	0.999
2. Fog oil	9	0.998
3. H_3PO_4 $180^o \pm 1^o$	14	0.997
4. Forward angles 0.266 micron wavelength	10	0.960
5. Forward angles 1.06 micron wavelength	6	0.966
6. Polarization 0.266 micron wavelength	16	0.899
7. Polarization 10.30 micron wavelength	2	0.346

Table 2. Optimally Selected Subsets of the Baseline Case

Number of Measurements	Significant Eigenvectors	Fraction of Recoverable Information
40	14	0.997
30	14	0.999
20	12	0.999
16	10	0.994
12	11	0.999
6	6	0.971

Returning to the baseline case, we now consider the results of optimal subset selection according to the optimization technique described in section 3.2. Table 2 is a summary of recoverable information fraction results for several optimal subset sizes. The number of significant eigenvectors, and thus "pieces of information" by Twomey's definition, stays the same or decreases with decreasing number of kernels or measurements; however, the recoverable information fraction stays very close to 100 percent until only 12 of the original 40 measurements are retained. The large fraction of recoverable information available in these subsets indicates that the optimal subsets have been closely approximated. A list of the baseline wavelengths and the subsets is given in appendix A, table A-1. The distributions produced by direct inversion of these subsets are further discussed in section 4.2.2.

4.1.3 Experimental Implications.

Selection of an optimal kernel set is, in essence, selection of a set of measurements to be made to obtain data for inversion. While the kernel sets tested were not exhaustive, a variety covering several plausible experimental approaches were tried with the backscatter set offering the most promise. It was, therefore, selected as the set to be optimized. Some of the experimental concepts tested with the eigenanalysis of the covariance matrix were forward scattering using 40 wavelengths, near-forward scattering with 40 wavelengths, a mixture of measurements made at different angles and wavelengths, plus the cases enumerated in section 4.2.2. The forward scattering approaches showed that only one or two significant eigenvectors ("pieces of information") could be obtained. They were, therefore, omitted from further consideration.

Table 1 shows the number of significant eigenvectors and the fraction of recoverable information for the various experimental approaches. The first observation of interest is that the backscatter measurement at a variety of wavelengths contains essentially all the information for phosphoric acid, water fog, and fog oil aerosols with the stated size distribution. The forward differential scattering measurements at 0.266 and 1.060 microns contain slightly less recoverable information and the polarization measurements significantly less.

As there are only 14 independent "pieces of information" contained in the 40 measurements made at different wavelengths, it is desirable to reduce the number of measurements as much as possible while still retaining the available information. Table 2 shows how the recoverable information varies as the number of measurements is reduced using the algorithm described in section 3.2. To retain all available information, a minimum of 12 measurements at different wavelengths is required; these are listed in table A-1 of appendix A. Thus, out of a set of backscatter measurements at 40 wavelengths, 12 have been selected as the minimal, optimal set. Fewer measurements means a loss in information.

A sensitivity analysis was performed using the optimal twelve wavelengths to see how changes in the particle size distribution affected the inversion results (see appendix B, figures B-1 - B-5). The significant result is that size distributions with smaller average diameters can not be accurately inverted from the data that is available at these wavelengths. This will represent a severe experimental handicap as the wavelength range from 0.266 micron to 10.30 microns was covered in the selection process. There are three possible ways out of this problem that should be investigated; find a different combination of experimental parameters that contains information on smaller particles, obtain shorter wavelength lasers, or try tightly constrained fits to the ill-conditioned experimental data. All of these approaches have obvious problems.

The backscatter measurements at the twelve wavelengths chosen enable one to obtain particle size distributions with means and standard deviations similar to the baseline case. Distributions with larger means and standard deviations are also experimentally accessible. However, data from smaller particles are difficult to invert using these measurements.

4.2 Inversion Results.

4.2.1 Test Case Description.

The baseline kernel set of section 4.1 was reduced to 12 members by optimization to provide a standard set of kernels upon which the various inversion techniques could be tested. Experimental error was simulated by generating

normally distributed random numbers with mean zero and standard deviation equal to an error level of either one or ten percent.

4.2.2 Test Case Results: Four Methods of Inversion.

The results for constrained linear inversion, Backus-Gilbert synthesis, Landweber iteration, and direct inversion are shown in figure B-6 for intensity data with no error. Notice that although the returned points are connected in the figure, only the direct inversion method has the capability to deliver the value of the inverted function at virtually any ordinate value. That is, the constrained linear, Backus-Gilbert, and Landweber techniques all return a limited number of points, with difficulty of inverting increasing as the number of returned points increases, while the direct method gives, in essence, a formula for computing the returned function at any point. Ten evenly spaced radius values in the range of interest were returned for Backus-Gilbert, Landweber, and constrained linear inversions.

The form of the kernel matrix for such a limited number of radius points must be considered. The integrals of smooth kernels involving, for example, simple exponential expressions, can be approximated using numerical quadrature techniques with relatively few points. Mie kernels, however, are typically not smooth in the regions of interest, and require many integration points for accurate evaluation. Backus-Gilbert, Landweber, and constrained linear inversion invert the matrix **A*A**, which is a square matrix with order equal to the number of returned points, where **A** is the quadrature weighted kernel matrix. Clearly, it is not acceptable to just perform the inversion for a large number of returned points; rather, special treatment of the kernel matrix is necessary. Each element a_{ij} of the kernel quadrature matrix **A** is given by

$$a_{ij} = \int_{r_j - \Delta/2}^{r_j + \Delta/2} \mathbf{K}(\lambda_i, r)\, dr \qquad (42)$$

where r_j is the jth radius or returned point, and Δ is the ordinate spacing between the returned radii. The integrals in equation 42 are each evaluated with the appropriate one-tenth of the 500 radii points.

Both direct and Landweber inversion give good results for the error free case. Constrained linear inversion and Backus-Gilbert show some spurious oscillation in the returned function at radius values in the lower end of the radius range. The quality of direct and Landweber results is maintained for measurement data with one percent simulated noise as shown in figure B-7. Backus-Gilbert results still show an erroneous tail for the smaller radii with good peak tracking for one percent noise, while constrained linear inversion continues to give adequate peak tracking with oscillations for smaller radii. Figure B-8 summarizes inversion results for a ten percent noise level in the measurement data. Landweber iteration gives the most reasonable approximation of the actual distribution. Direct inversion results are generally similar to the Landweber results, with some added oscillation at the larger radii. Constrained linear inversion still has problems inverting at smaller radii, but the overall solution is also acceptable. Backus-Gilbert results retain the left tail for smaller radii, and produce a peak and right tail similar to Landweber and direct inversion results.

The principal advantage of the direct inversion method is its straightforward approach to evaluating measurement error effects. Where constrained linear inversion and Landweber iteration require incorporation of arbitrary smoothing constraints, direct inversion gives a mathematically rigorous criterion for eliminating oscillatory components as a function of anticipated measurement error. Where Backus-Gilbert attempts to construct linear combinations of the kernels such that Dirac delta functions are approximated, direct inversion makes use of the eigenfunctions that maximize variance and are orthogonal by definition. The direct-inverted function also has the advantage of radius resolution as fine as the resolution used for the master set of kernels; that is, the numerical approximation of integrals of oscillatory functions by quadrature with only a few points is not necessary.

4.2.3 Direct Inversion Sensitivity Results.

Sensitivity analysis of direct inversion of the baseline 40 and the standard subset of 12 measurements was performed to gain a better understanding of the limitations and strengths of the direct inversion method. We have already considered some interesting parameter variations in previous sections. For

example, a summary of direct inversion results for the various error levels discussed in section 4.2.2 is given in figure B-9. The effect of the number of measurements decreasing from 40 to six, briefly described in table 2, is illustrated in figure B-10 . Figure B-1 compares inversion with optimal kernel sets for each of the three materials for a ten percent measurement noise level. Each of the materials produce similar inverted results since the number of significant eigenvectors and the recoverable information fraction are similar for the three materials.

We have seen a subset of 12 measurements that contains most of the information about the lognormal size distribution with geometric mean diameter d_g of 1.6 and geometric standard deviation σ_g of 1.2. Recalling the optimization scheme of section 3.2, notice that the kernels are selected without regard to the particle size distribution. The kernel covariance matrix determines the optimal measurements. The particular size distribution only enters into computing the recoverable information fraction. Since the actual particle size distribution is not known, there is a need to understand how varying the size distribution affects inversion quality. The standard subset of 12 measurements was regenerated using identical kernels, but varying particle size distributions. All size distributions were lognormal, and only one of the parameters σ_g or d_g was varied from the standard values for each of the sensitivity cases. Figures B-2 and B-3 the standard distribution and the inverted results as well as two actual-inverted pairs for distributions with decreased geometric mean diameter. In figure B-2, d_g is 1.2, and in figure B-3, d_g is 1.0. Although the same ten eigenvectors are used in each inversion, results are significantly degraded as the geometric mean diameter decreases. The recoverable fraction decreases dramatically as d_g decreases. The effects of increasing or decreasing the geometric standard deviation are shown in figures B-4 and B-5. In figure B-4, σ_g is 1.4, and in figure B-5, σ_g is 1.1. The recoverable fraction data indicates that although the inversion results are degraded, the effects are not as severe as when the peak is shifted to lower radii. The ten eigenfunctions used to construct f(x) are shown in figures B-11 through B-20. These eigenfunctions do not show much structure in the lower radius region, and since by equation 9, successful inversion requires forming linear combinations of the eigenfunctions to resemble the desired inverted function, good inversion results in the lower radius region are not expected.

The upper radius limit for integrating the size distributions was arbitrarily set at 1.3 microns for the baseline case, with the idea that the value of the distribution at 1.3 microns is greatly diminished from the peak value occuring at 0.8 micron. Direct inversion results for this region show a tail on the right that gets progressively worse as the error level in measurements increases. The sensitivity to upper range limit was tested by adding a section of 0.2 micron width on to the upper end of the radius interval. The number of points at which the kernels were evaluated was proportionately increased to 577, and the standard optimal 12 measurements were correspondingly recomputed and subsequently inverted. The results for ten percent noise for the baseline and revised radius range cases are given in figure B-21. For the noise-free case, the number of significant eigenvectors for the extended range kernels increased to 11, but the recoverable fraction exceeded 1.0, indicating that perhaps the error level is higher than the expected 0.1%. Note that the optimized kernels for the 0.001 to 1.3 micron range are not necessarily the optimal kernels for the 0.001 to 1.5 micron range. The important finding from this case is that the limits of the integrations can profoundly affect inversion results. The correlation between the two kernels could be large over one radius interval, yet quite small for a different and perhaps more interesting radius interval.

The effects of changing the form of the actual distribution provide some additional insight into the direct inversion technique. A bimodal distribution composed of a lognormal with σ_g of 1.2 and d_g of 1.6 added to a lognormal with σ_g of 1.3 and d_g of 3.0 was used to generate synthetic backscatter measurements which were then input to the direct inversion method. The radius range extended from 0.001 to 3.0 microns. For the baseline 40 wavelengths for H_3PO_4 smoke, there were 21 significant eigenvectors for noise free data, giving a recoverable fraction of 0.993. The optimization technique was applied to the 40 kernels, and the set of 25 optimal kernels was tested for inversion quality at the several levels of error. The selected kernels, given in table A-2, reflect a preference for more medium and long wavelength kernels for this radius range. For the optimal-25 subset, there were 21 significant eigenvectors, giving a recoverable fraction of 0.997. The twentieth eigenvector adds a good portion of the information fraction, indicating that for low error levels, keeping fewer than 20 eigenvectors would not provide sufficient structure to produce a desirable inversion result. Figure B-22

gives the bimodal distribution and the noise-free, one percent, and ten percent measurement error direct inversion results. Figure B-23 gives inversion results for a lognormal distribution, with d_g larger than the d_g of the baseline case, in the same radius region as the bimodal distribution of figure B-22. Note that the right tails of the returned distributions do not suddenly turn up the way they do for the cases inverted in a smaller radius range. The ten percent noise results show a serious degradation of results, with a recoverable fraction of only 0.660. Sensitivity to radius range, bimodal shape, and numerical integration procedure will provide interesting insights as investigation into the direct inversion method continues.

5. CONCLUSIONS AND RECOMMENDATIONS

The information content of a set of measurements has been the focal issue of the Inversion Technique Evaluation study. The direct method of inversion has been developed into a tool for determining the information content of a set of kernels as well as a complete method of inversion, including prediction of experimental error propagation in the solution. Unpolarized backscatter intensity measurements for small incident wavelengths were found to be the most desirable, with respect to information content, when compared to transmission data, polarization data, angular scan data, and wavelength data for various fixed angles. The direct inversion method identifies how many of the orthonormal eigenfunctions should be taken for any given measurement set and level of experimental noise. The number of measurements may then be reduced to the number of eigenfunctions, and the process repeated to assure that the number of significant eigenvalues and the recoverable information are not significantly degraded. The eigenfunctions, when plotted as a function of radius, provide a clear representation of the radius regions in which successful inversion can be expected. Results are excellent for inversion of the optimized measurements by the direct inversion method for experimental noise levels of one and ten percent. Landweber iteration also produces excellent results, but adds no insight into the physical processes involved that help to determine under what conditions inversion may be successfully applied. Backus-Gilbert synthesis and constrained linear inversion were found to be lacking in both inversion quality and ease of physical interpretation.

The eigenfunctions examined point out that distributions with larger particle sizes can be inverted more successfully than those with small particles. No structure is apparent for smaller radii, and that lack of structure causes difficulties when requiring a linear combination of the eigenfunctions to sum to a smooth function over the entire radius range of interest. It would be interesting to delete the lower portion of the radius interval, reoptimize, and invert to see if improvement in results was obtained as the no-information, no-structure portions of the original eigenfunctions were deleted. Shorter wavelengths would also help inversion of smaller size distributions, but are not available for measurements. An understanding of why each of the methods performs as well or as poorly as it does would offer further insight into kernel selection and the strengths and limitations of each of the methods. Further sensitivity analysis of the radius interval and particle size distribution is necessary to more fully understand kernel optimization for realistic laboratory conditions.

Developing a physical understanding of the effects of smoothing constraints could be important for kernels sets that may not contain much information, but must be inverted, and for cases in which something is known about the actual distribution. The relative merits of inversion with these smoothing constraints as opposed to a procedure such as parameter fitting could then be compared without the arbitrariness now prevalent in inversion techniques using smoothing constraints.

To summarize, the major conclusions of this study are:

- Excellent inversion results for the problem considered here are achievable using the direct or the Landweber methods on measurement data with noise levels to 10%.
- The information content of a set of measurements and error propagation predictions are also available from the direct inversion method.
- The direct inversion method provides a physical understanding of kernel dependencies and their effect on inversion quality.
- A quantitative measure of the maximum information available from a given set of measurements is available from the direct inversion method.

- A group of candidate measurements may be systematically reduced to an optimal subset which retains a known fraction of the information present in the larger set.

- Unpolarized backscatter measurements at small wavelengths have the highest information content of the measurement sets analyzed.

The major recommendations for further study are:

- An understanding of the effects of the radius interval used for integration should be more thoroughly developed.

- Incorporation of a priori knowledge or smoothing constraints into the inversion process should be further investigated.

- Further analysis of why each of the four methods performs well or poorly for a given data set should be performed.

- Inversion of bimodal distributions requires further investigation.

LITERATURE CITED

1. Twomey, S. Information Content in Remote Sensing. Applied Optics, Vol. 13, p 942-945 (1974).

2. Twomey, S. An Introduction to the Mathematics of Inversion in Remote Sensing and Indirect Measurements. Elsevier Scientific Publishing, New York, New York. 1977.

3. Landweber, L. An Iteration Formula for Fredholm Integral Equations of the First Kind. American Journal of Mathematics, Vol 73, p 615-624 (1951).

4. Strand, O. N. Theory and Methods Related to the Singular-Function Expansion and Landweber's Iteration for Integral Equations of the First Kind. Siam Journal of Numerical Analysis, Vol 11, p 798-825 (1974).

5. Westwater, E. R., and Cohen, A. Application of Backus-Gilbert Inversion Technique to Determination of Aerosol Size Distributions from Optical Scattering Measurements. Applied Optics, Vol 12, p 1340-1348 (1973).

6. Westwater, E. R., and Strand,O. N. NOAA Technical Report ERL 309-WPL 34. A Generalized Inversion Program. November, 1974. UNCLASSIFIED Report.

7. Dave, J. V. Subroutines for Computing the Parameters of the EM-Radiation Scattered by a Sphere. IBM Document No. 360D-17.4.002, IBM Scientific Center, Palo Alto, CA. 1968.

BIBLIOGRAPHY

1. Cattell, R. Factor Analysis: An Introduction to Essentials I. The Purpose and Underlying Models. Biometrics, p 190-215 (1965).

2. Harman, H. H. Modern Factor Analysis. University of Chicago Press, 1960.

3. Henning, R. L. Determination of Aerosol Particle Size Distribution by Constrained Linear Inversion of Optical Measurements. Boeing Document No. D180-26229-1. 1980.

4. Henning, R. L. Comparative Evaluation of Optical Inversion Techniques. Boeing Document No. D180-26400-1. 1981.

5. Parks, J. M. Fortran IV Program for Q-Mode Cluster Analysis on Distance Function with Printed Dendrogram. State Geological Survey, University of Kansas, Lawrence, Kansas. 1970.

6. Parks, J. M. Cluster Analysis Applied to Multivariate Geologic Problems. Journal of Geology, Vol. 74, p 703-715 (1966).

7. Wilkinson, J. H. The Alegbraic Eigenvalue Problem. Clarendon Press, London. 1965.

APPENDIXES

APPENDIX A TABLES

APPENDIX B FIGURES

APPENDIX A

TABLES

Table A-1. The Optimal Subsets of the Baseline Case .001 - 1.3 Microns

Wavelengths microns	Subset of 30	Subset of 20	Subset of 16	Subset of 12	Subset of 6
0.266	X	X	X	X	X
0.524	X	X	X	X	X
0.782	X	X	X	X	X
1.040	X	X	X	X	
1.290	X	X			
1.550	X	X	X	X	
1.815	X	X	X		
2.075	X	X	X		
2.330	X	X	X	X	
2.590	X	X	X	X	
2.850	X	X	X	X	X
3.110	X	X			
3.335	X	X	X		
3.625	X	X	X	X	
3.880	X	X	X	X	
4.140	X	X	X	X	X
4.400	X	X			
4.660	X	X			
4.910	X	X	X	X	X
5.170	X				
5.430	X				
5.690					
5.950	X				
6.210	X				
6.470	X				
6.720	X				
6.980	X				
7.240	X				
7.500					
7.750					
8.020					
8.270					
8.530					
8.790	X				
9.050					
9.300					
9.560					
9.830					
10.075	X				
10.300	X	X	X		

Table A-2. The Optimal Subsets of the Baseline Case Extended .001 - 3.0 Microns

Wavelengths microns	Subset of 30	Subset of 20	Subset of 16	Subset of 12	Subset of 6
0.266	X	X	X	X	X
0.524	X	X	X	X	
0.782	X	X	X		
1.040	X	X	X	X	
1.290	X	X	X	X	
1.550	X	X	X	X	X
1.815	X	X	X	X	
2.075	X	X	X		
2.330	X				
2.590	X				
2.850	X	X	X	X	X
3.110	X	X			
3.335	X	X			
3.625	X				
3.880	X	X	X		
4.140	X	X	X	X	
4.400	X				
4.660	X	X	X	X	X
4.910	X	X			
5.170	X				
5.430	X				
5.690	X	X			
5.950					
6.210	X	X	X	X	X
6.470	X				
6.720	X				
6.980	X				
7.240	X	X	X		
7.500					
7.750					
8.020					
8.270					
8.530					
8.790	X	X	X	X	
9.050	X				
9.300					
9.560					
9.830					
10.075					
10.300	X	X	X	X	X

APPENDIX B

FIGURES

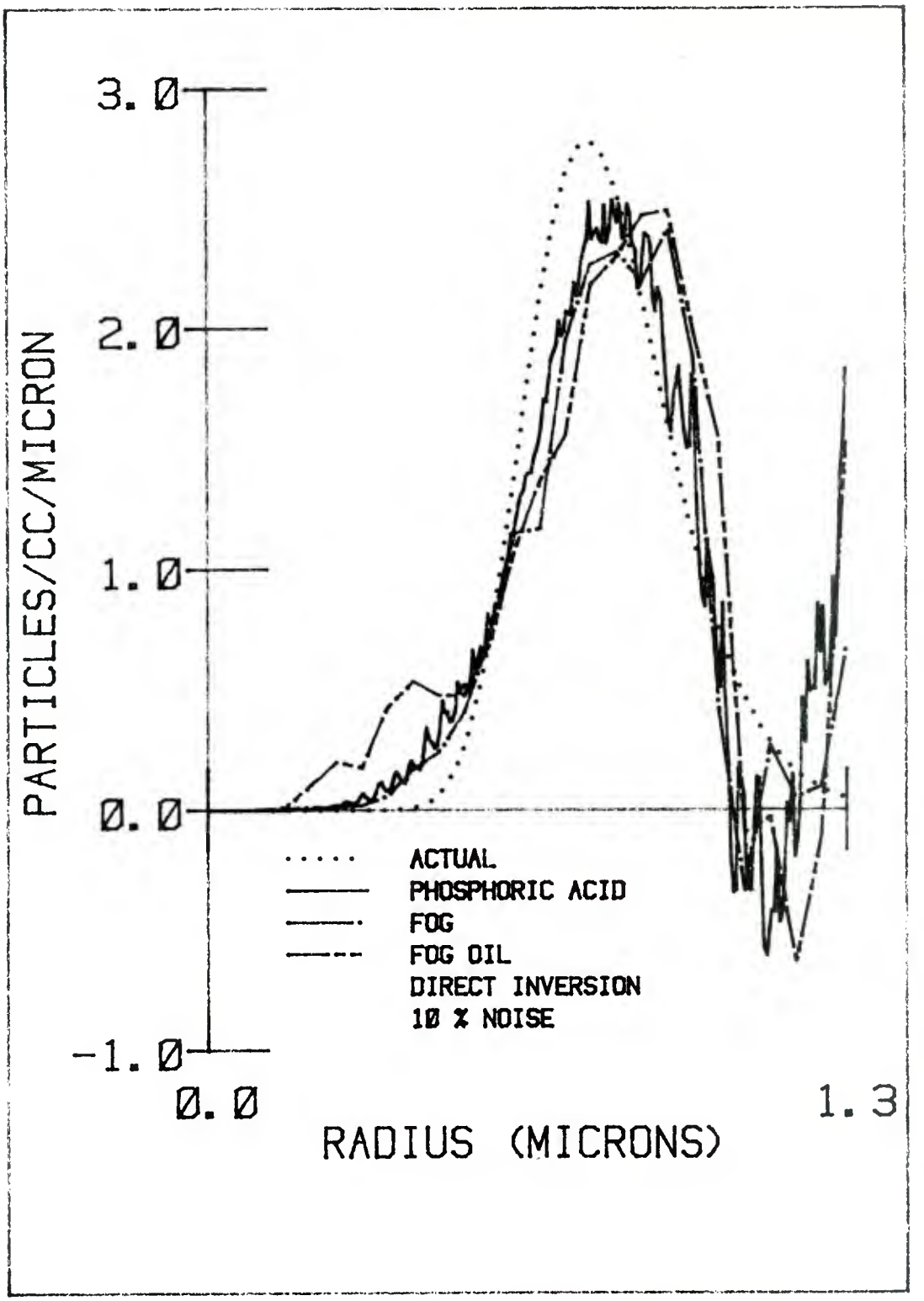

Figure B-1. Direction Inversion Results for Three Materials

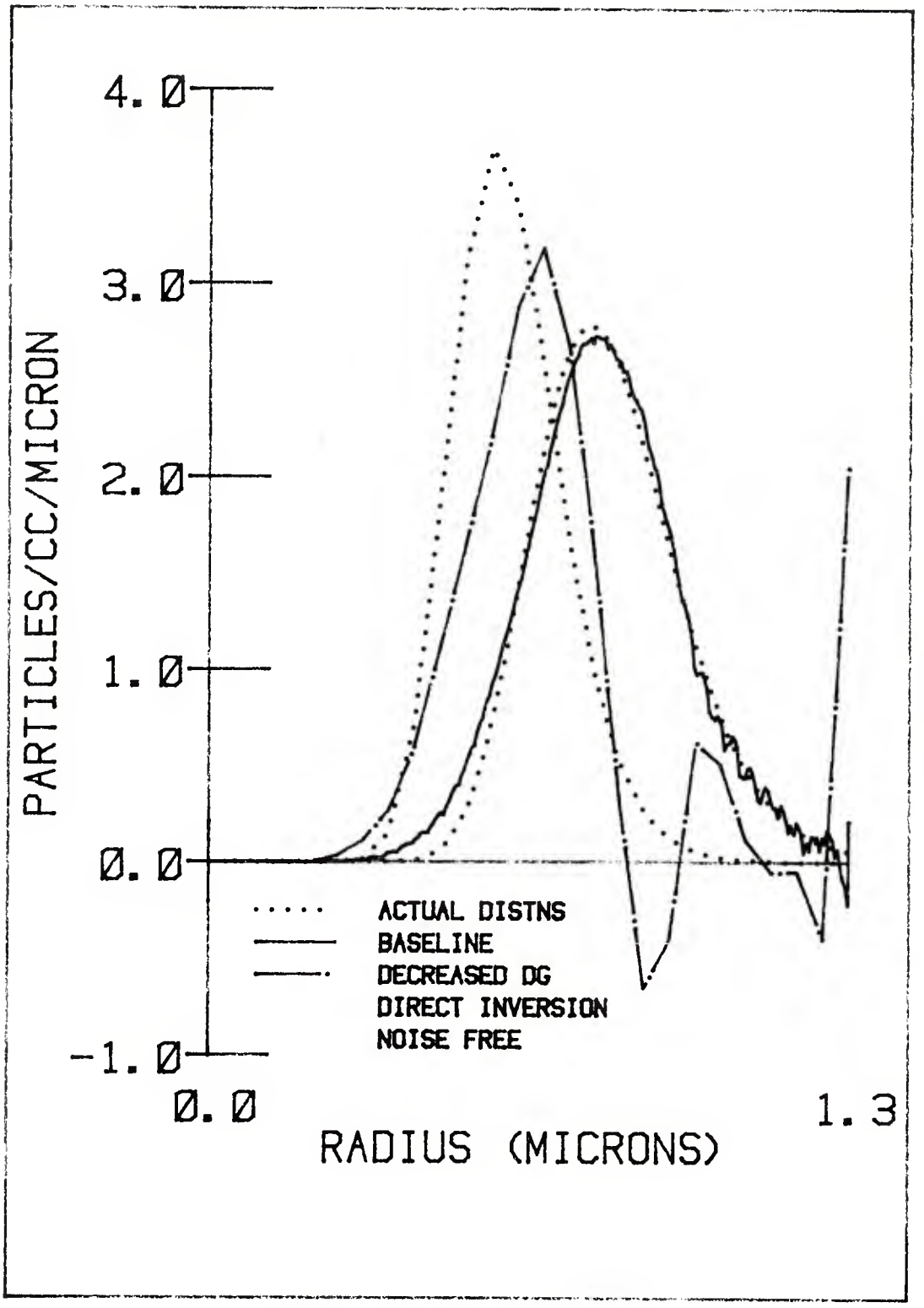

Figure B-2. Direct Inversion Results: Sensitivity to Decreased Geometric Mean Diameter $\sigma_g = 1.2$, $d_g = 1.2$ Recoverable Fraction = 0.894

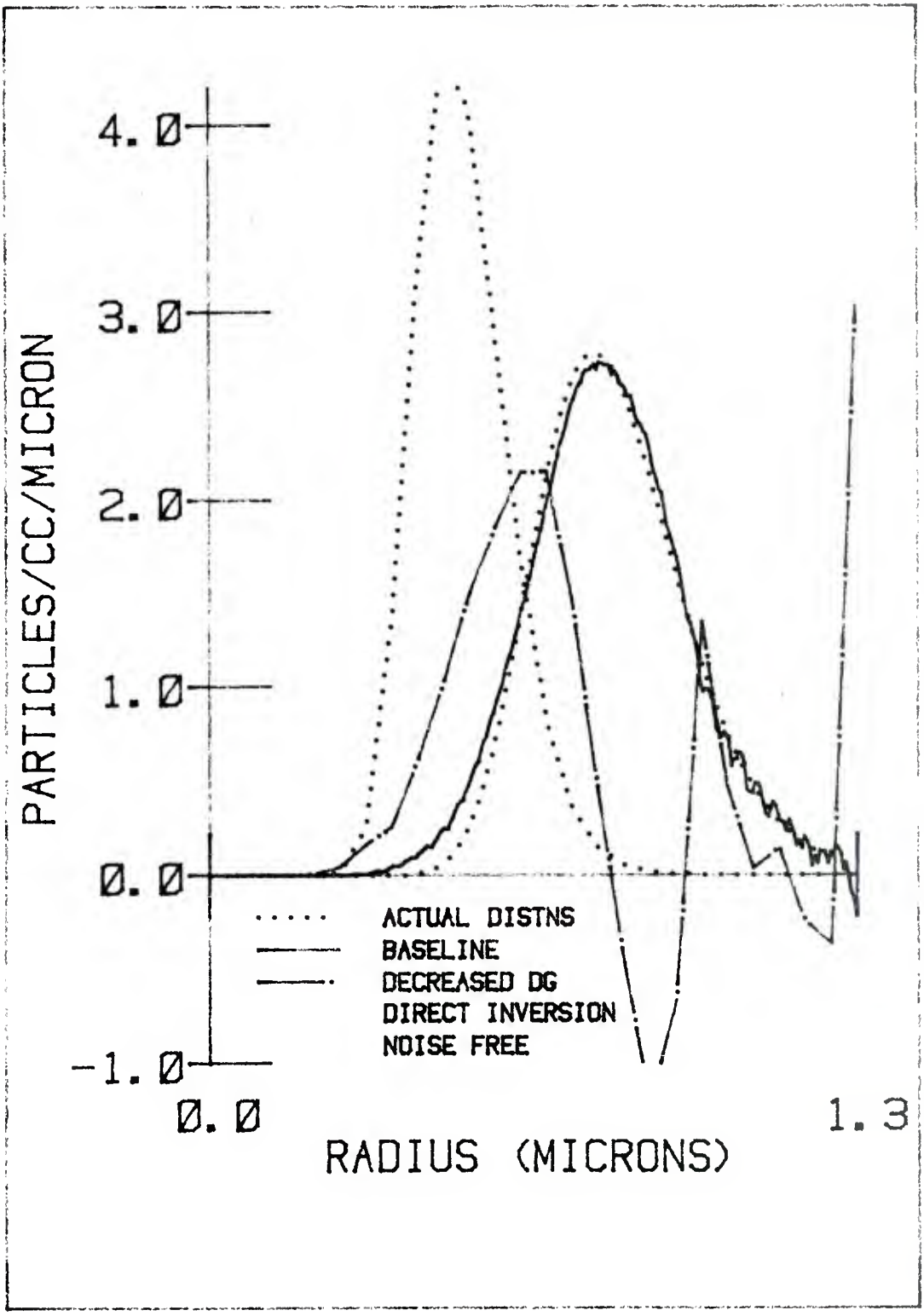

Figure B-3. Direct Inversion Results: Sensitivity to Decreased Geometric Mean Diameter $\sigma_g = 1.2$, $d_g = 1.0$ Recoverable Fraction = 0.630

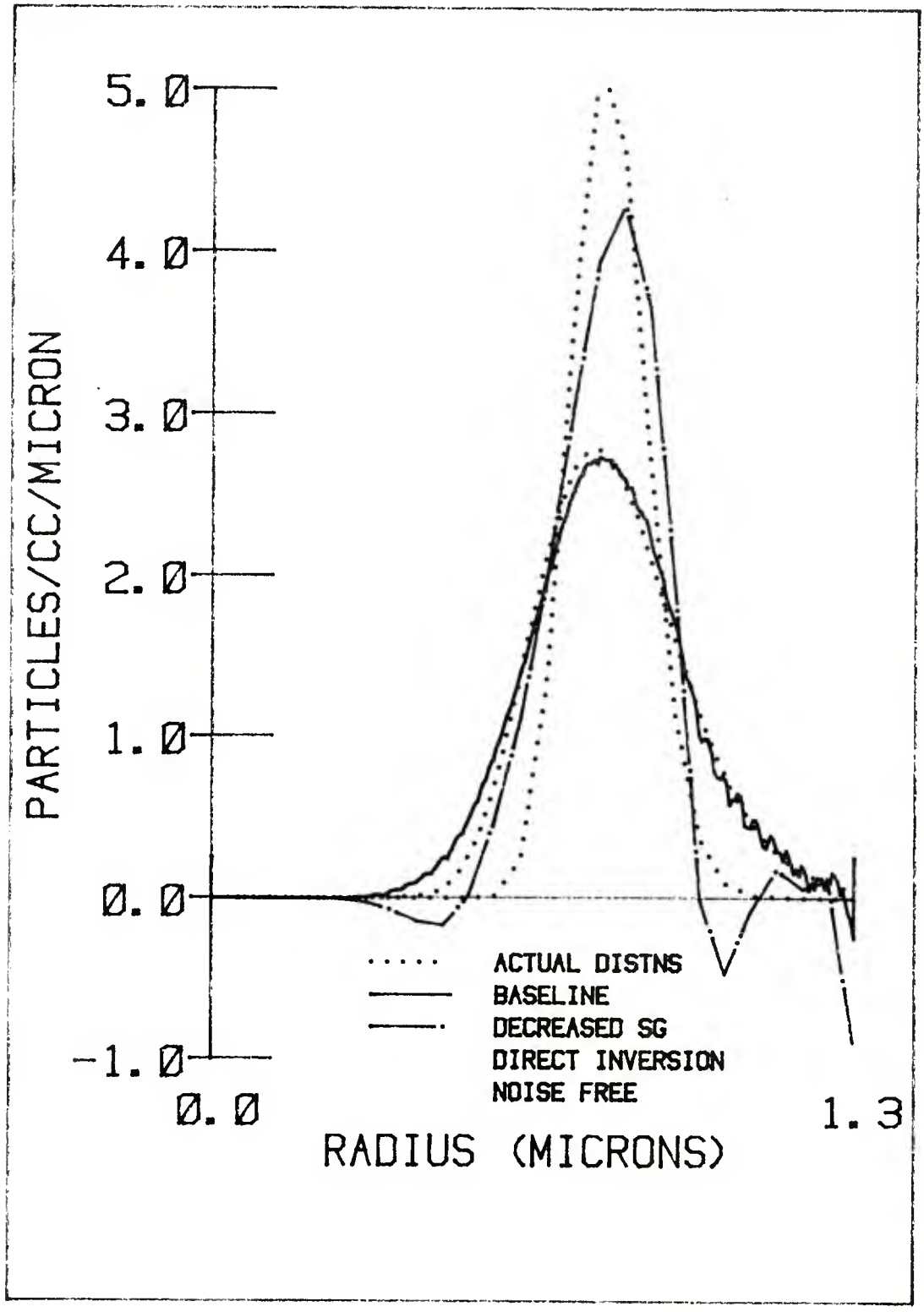

Figure B-4. Direct Inversion Results: Sensitivity to Decreased Geometric Standard Deviation σ_g = 1.1, d_g = 1.6 Recoverable Fraction = 0.960

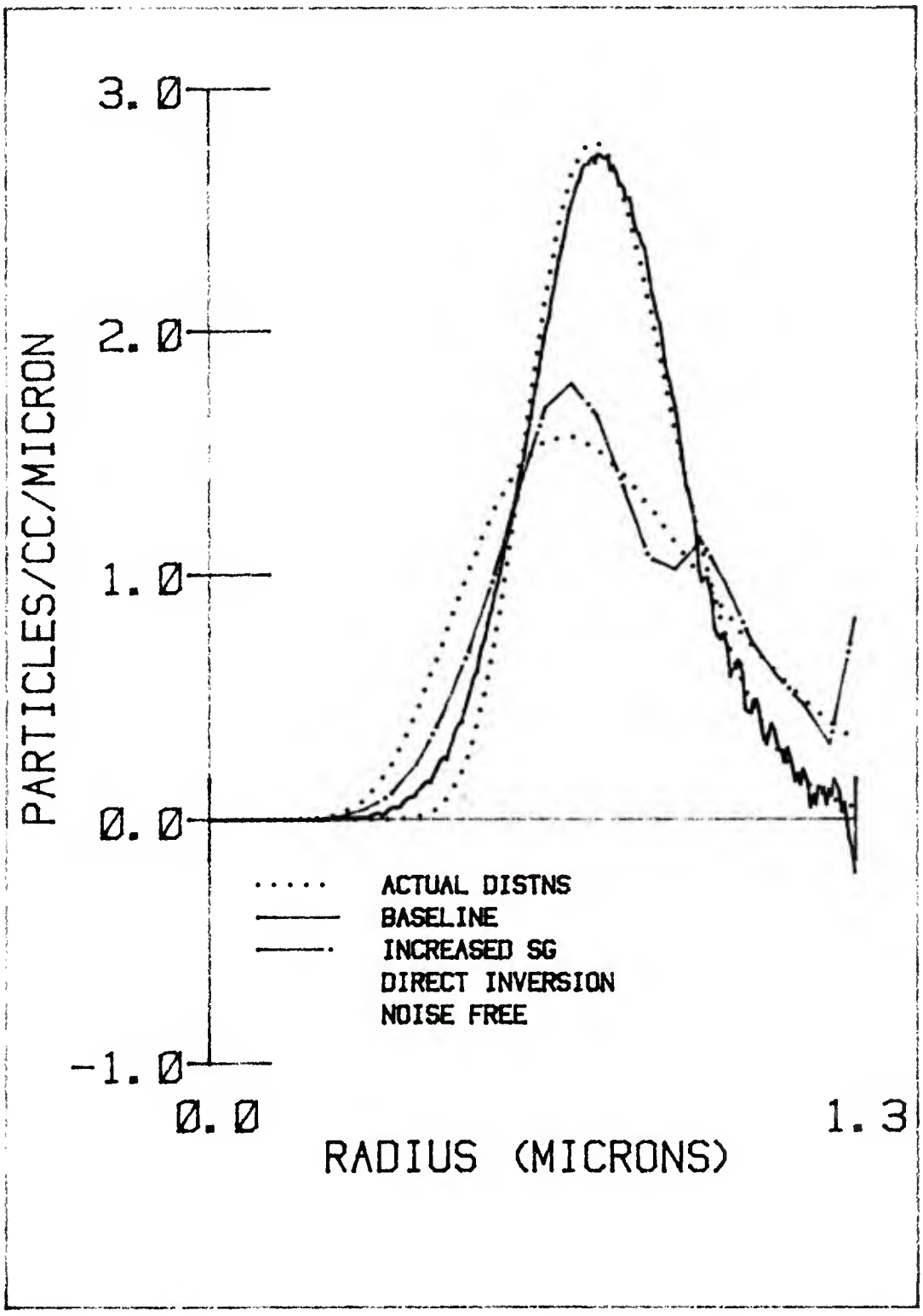

Figure B-5. Direct Inversion Results: Sensitivity to Increased Geometric Standard Deviation $\sigma_g = 1.4$, $d_g = 1.6$ Recoverable Fraction = 0.984

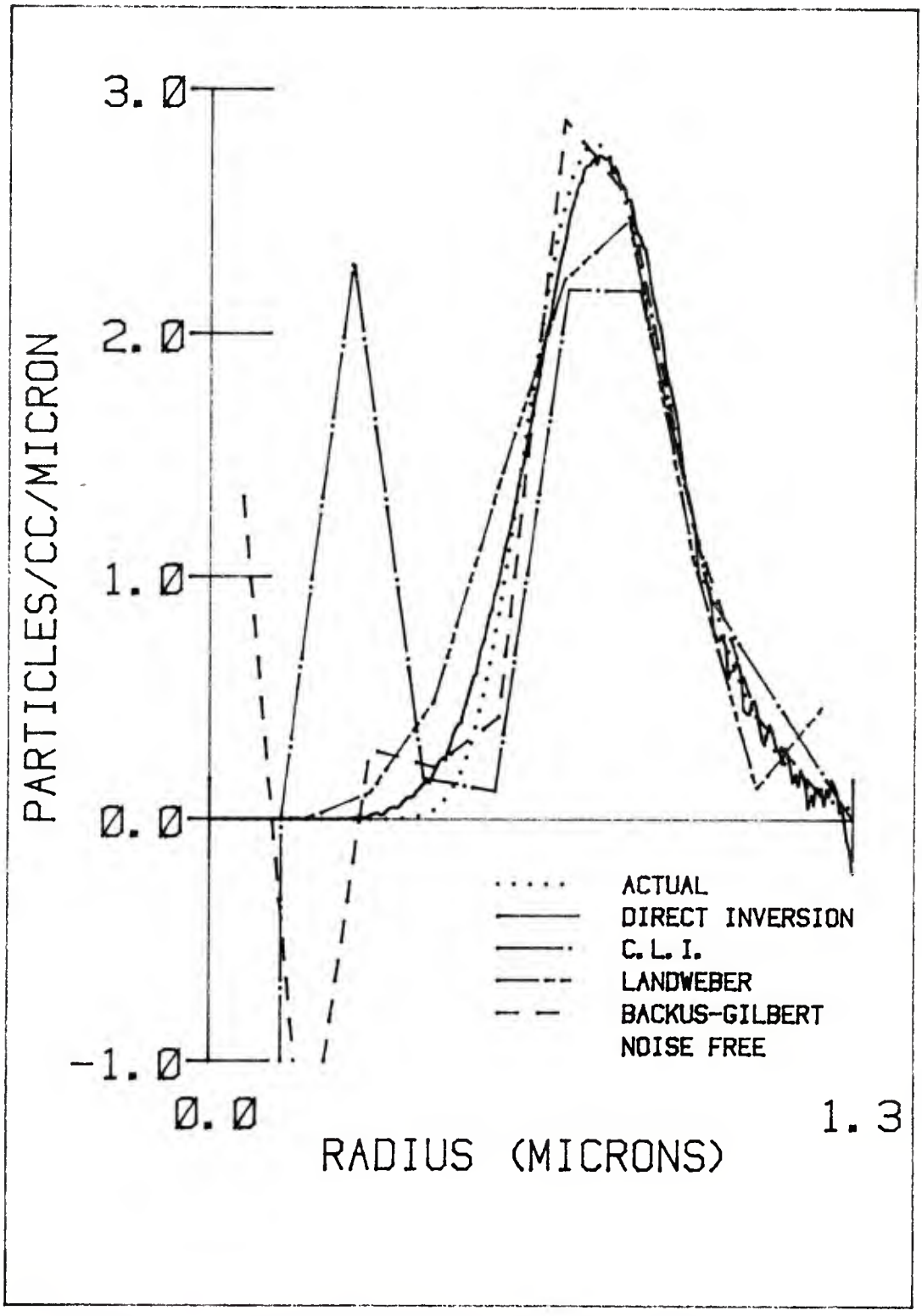

Figure B-6. Comparison of Results for the Four Inversion Methods: Noise Free

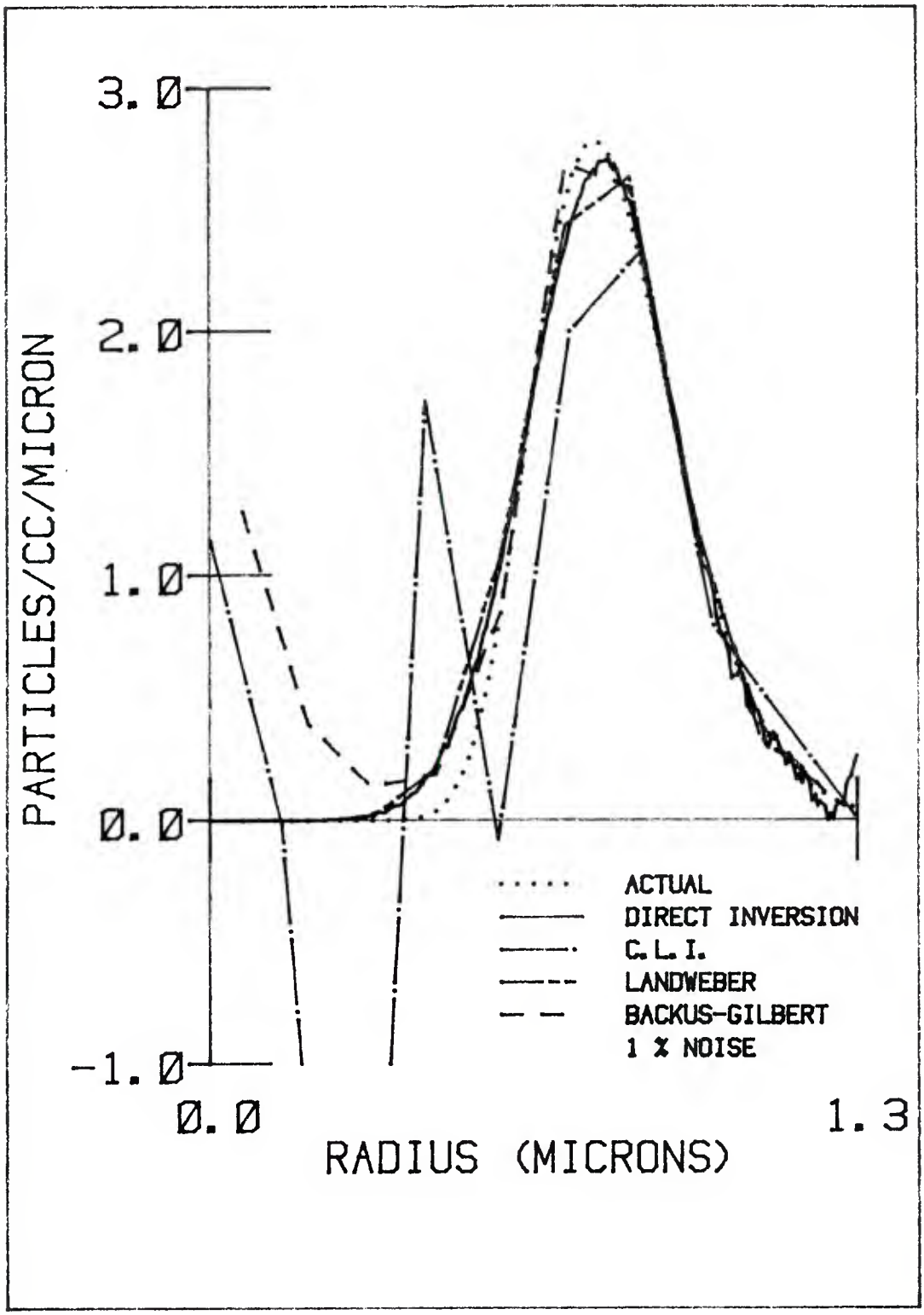

Figure B-7. Comparison of Results for the Four Inversion Methods
1 % Noise

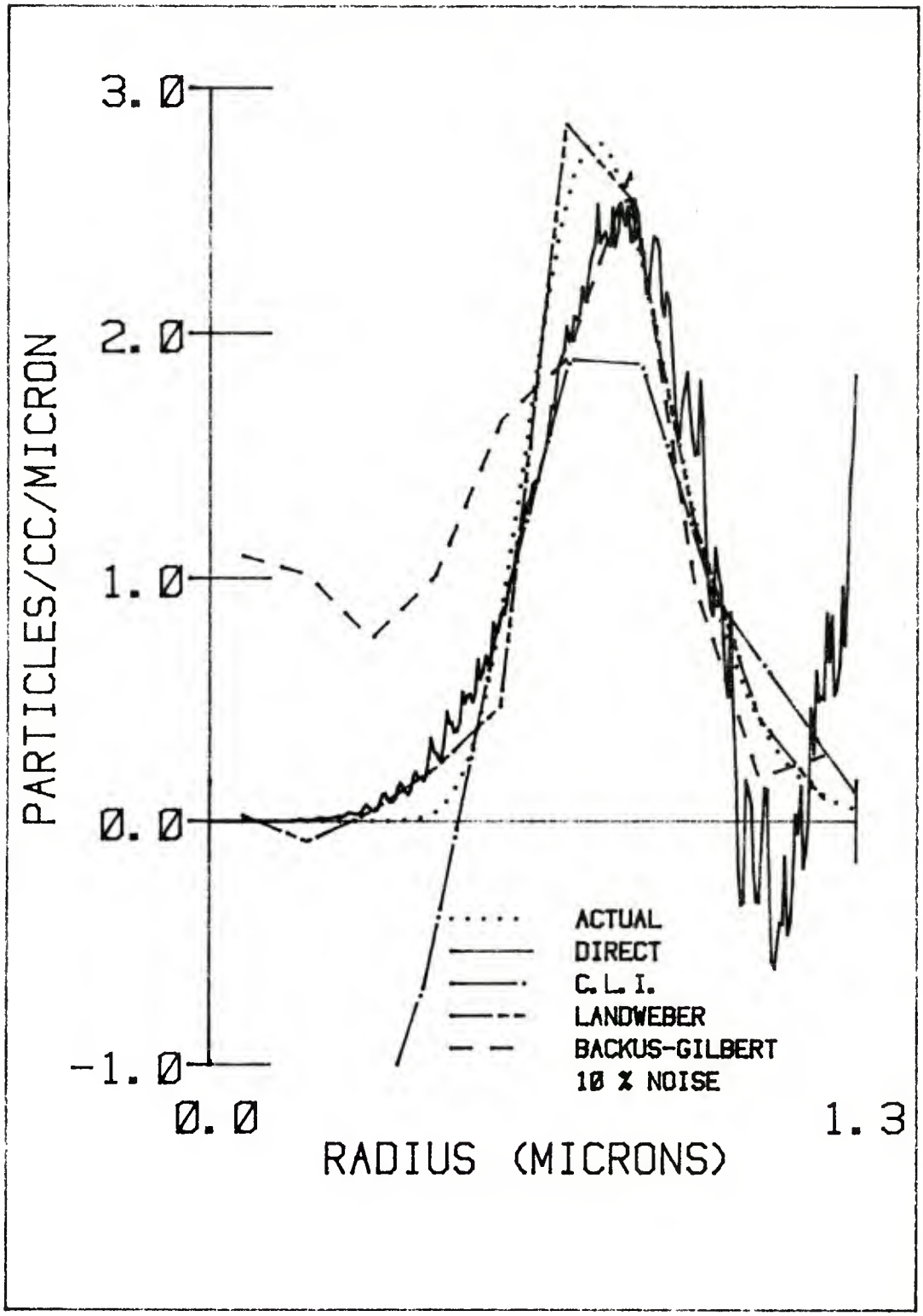

Figure B-8. Comparison of Results for the Four Inversion Methods: 10 % Noise

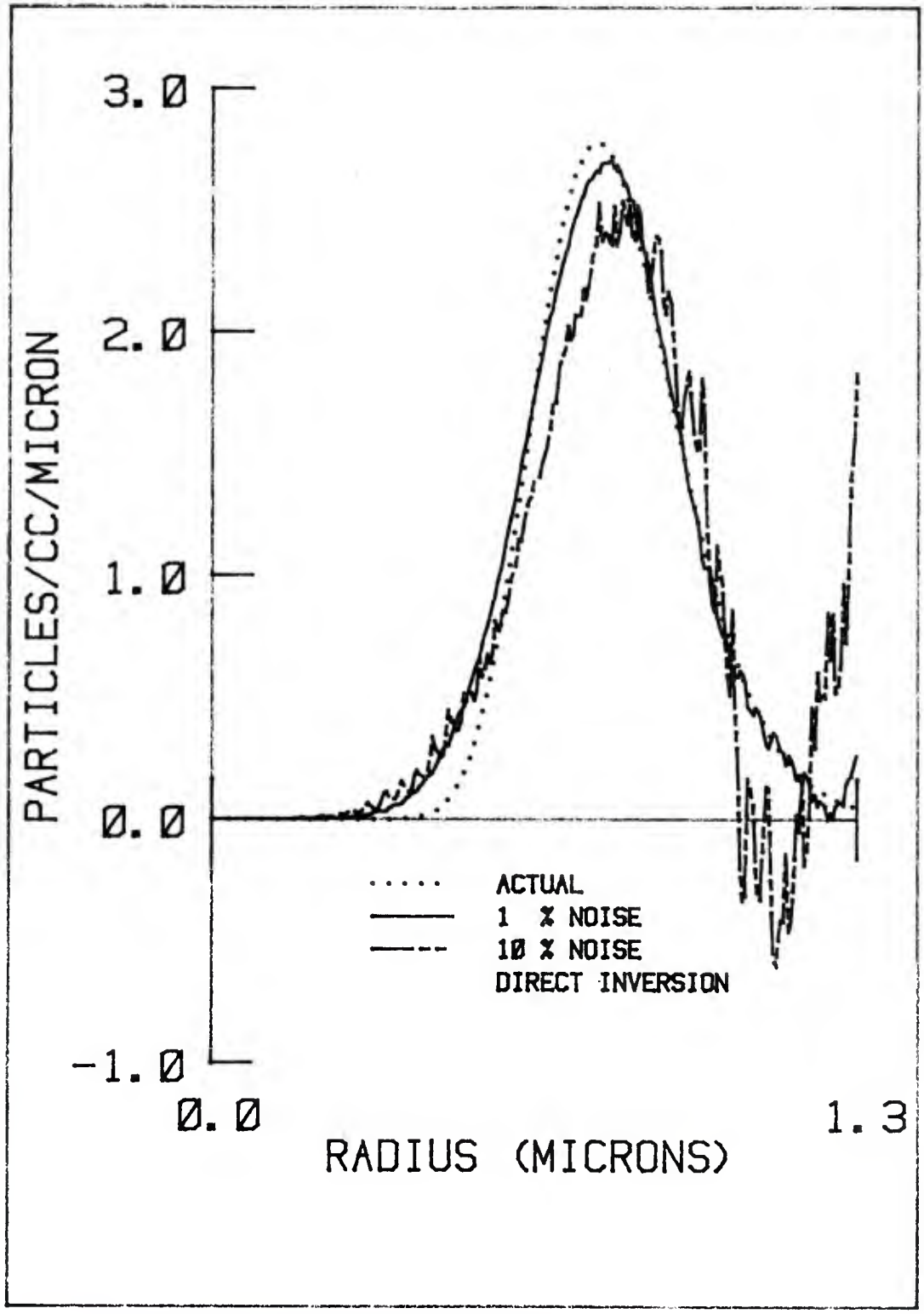

Figure B-9. Direct Inversion Results for Three Noise Levels

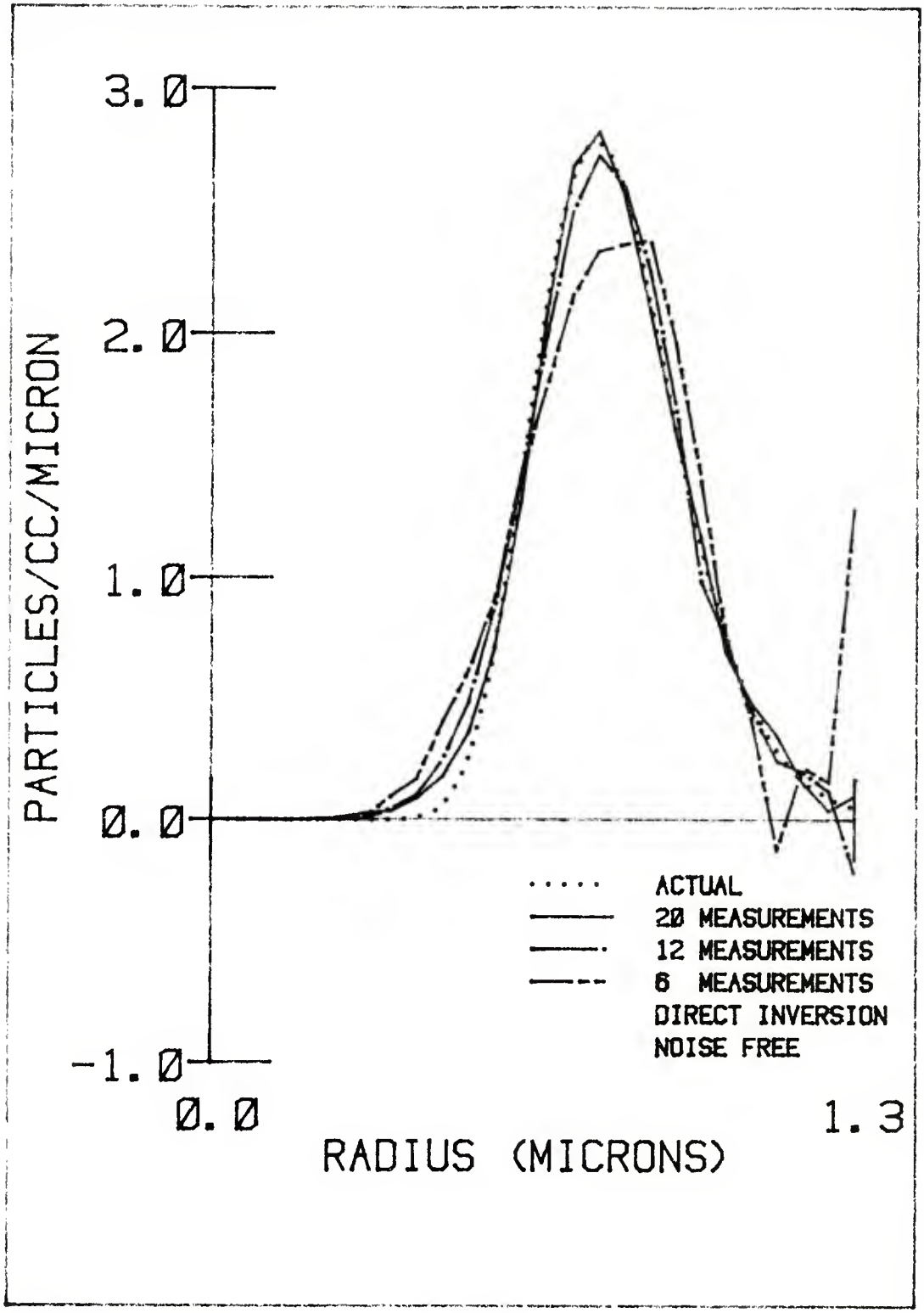

Figure B-10. Direct Inversion Results for Varying Number of Measurements

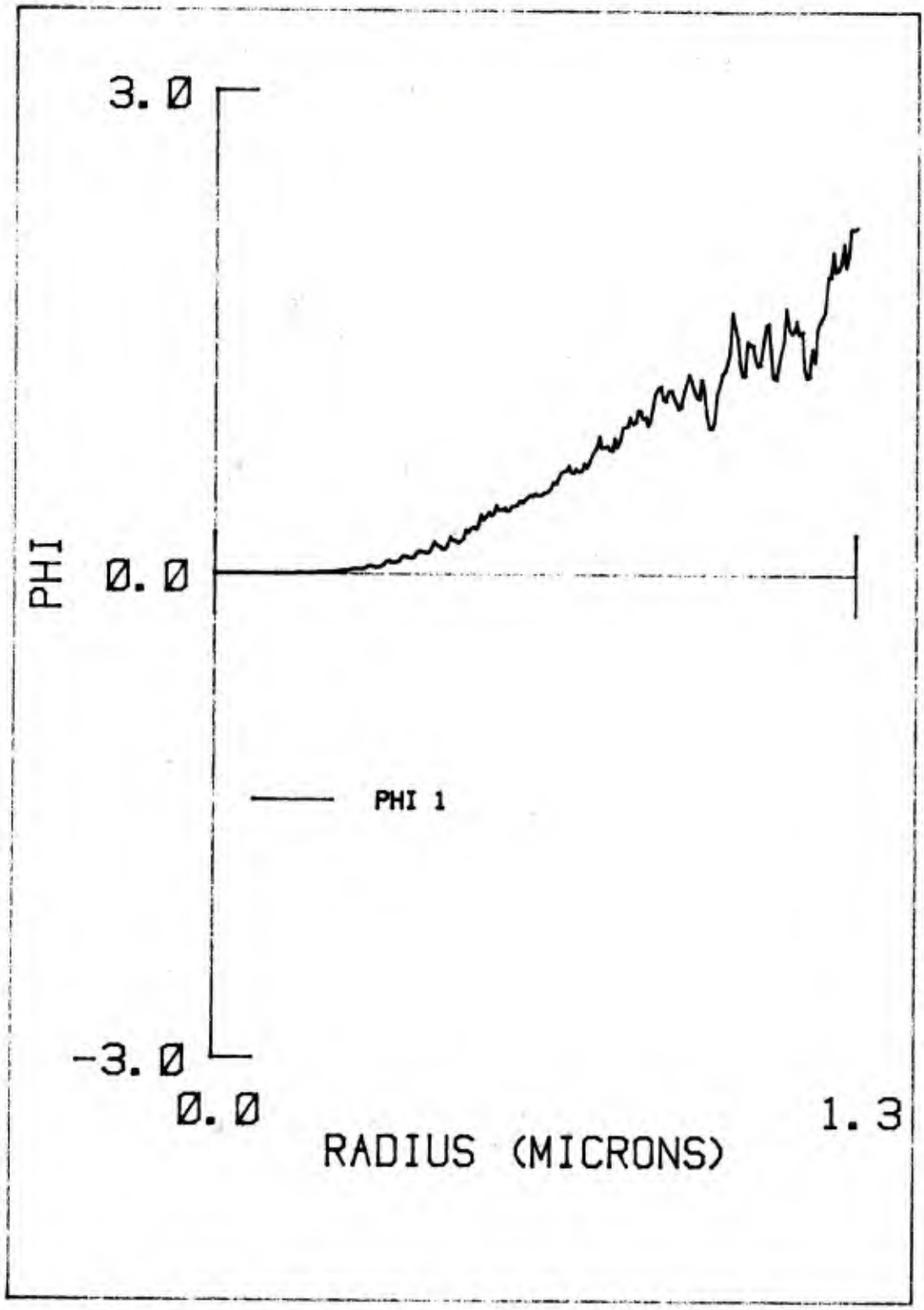

Figure B-11. The Ten Most Significant Eigenfunctions for the Baseline Case: ϕ_1

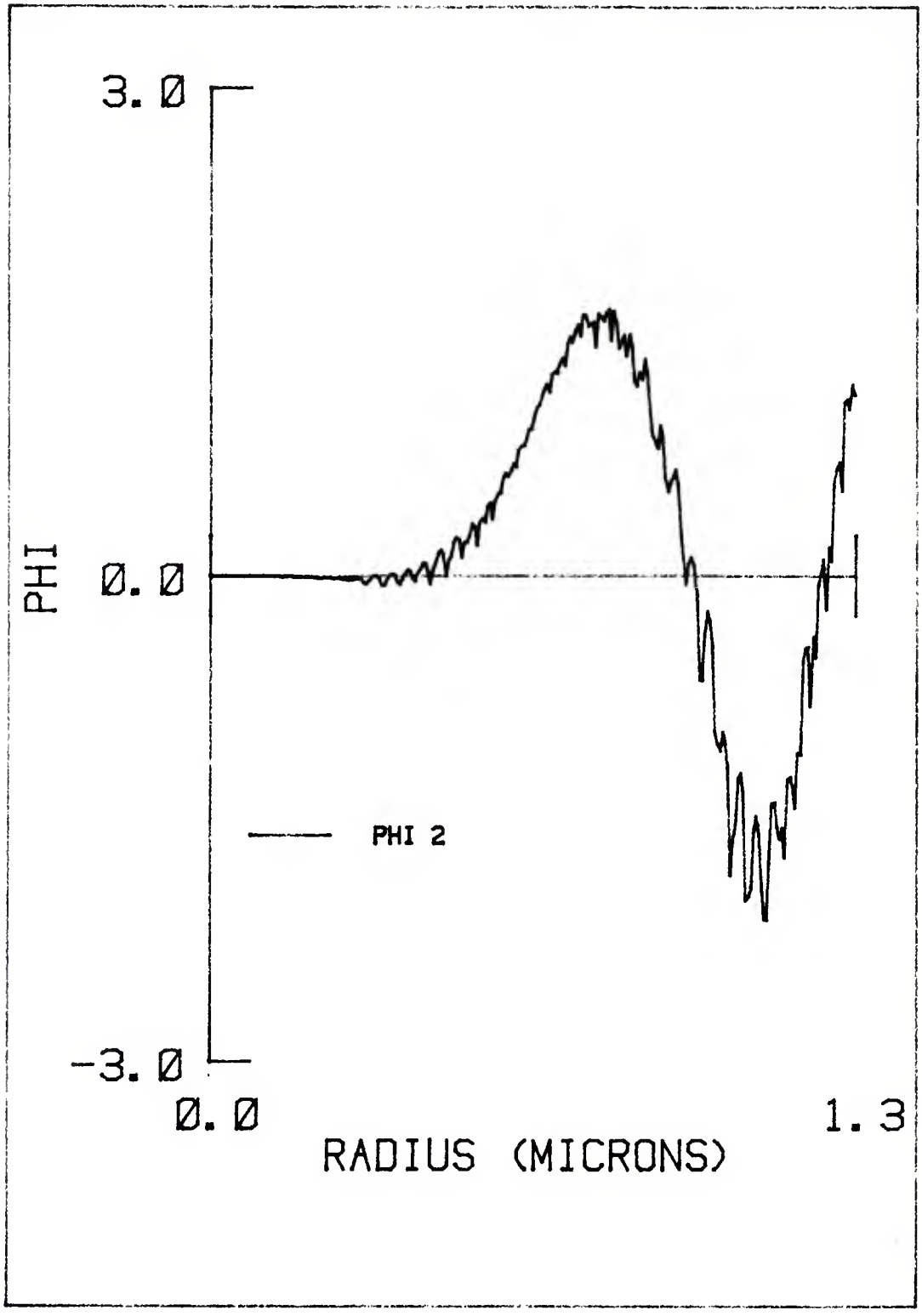

Figure B-12. The Ten Most Significant Eigenfunctions for the Baseline Case: ϕ_2

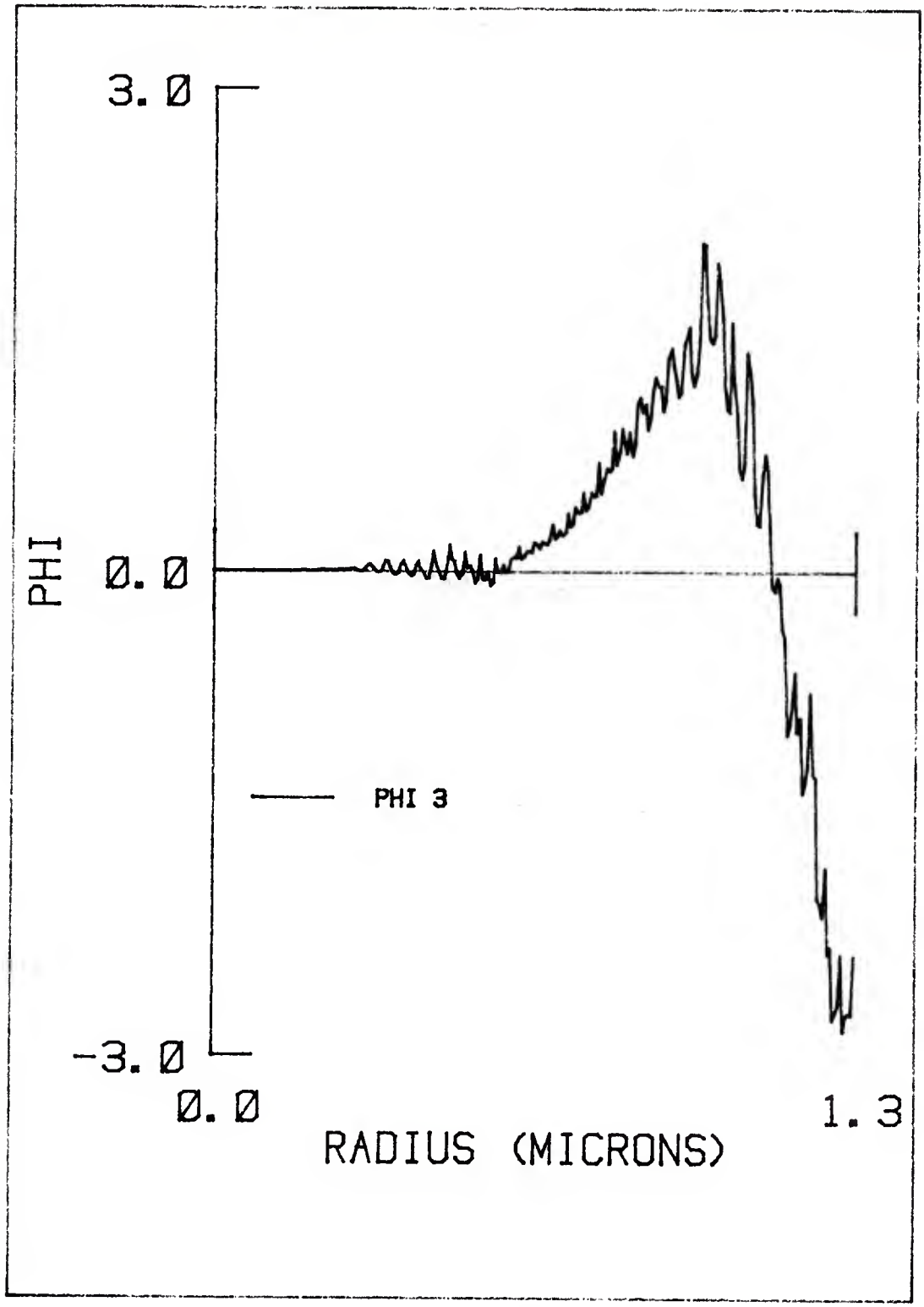

Figure B-13. The Ten Most Significant Eigenfunctions for the Baseline Case: ϕ_3

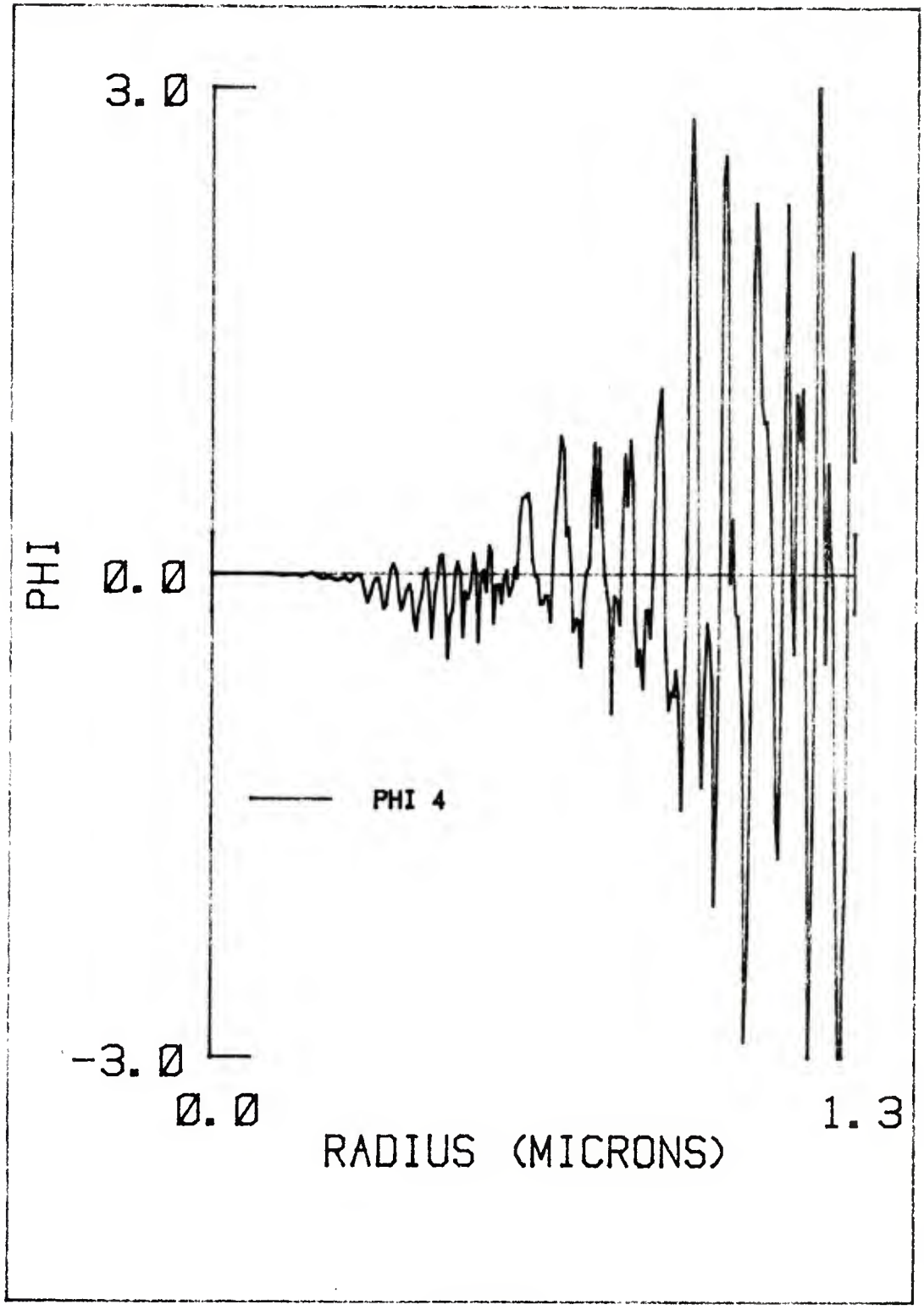

Figure B-14. The Ten Most Significant Eigenfunctions for the Baseline Case: ϕ_4

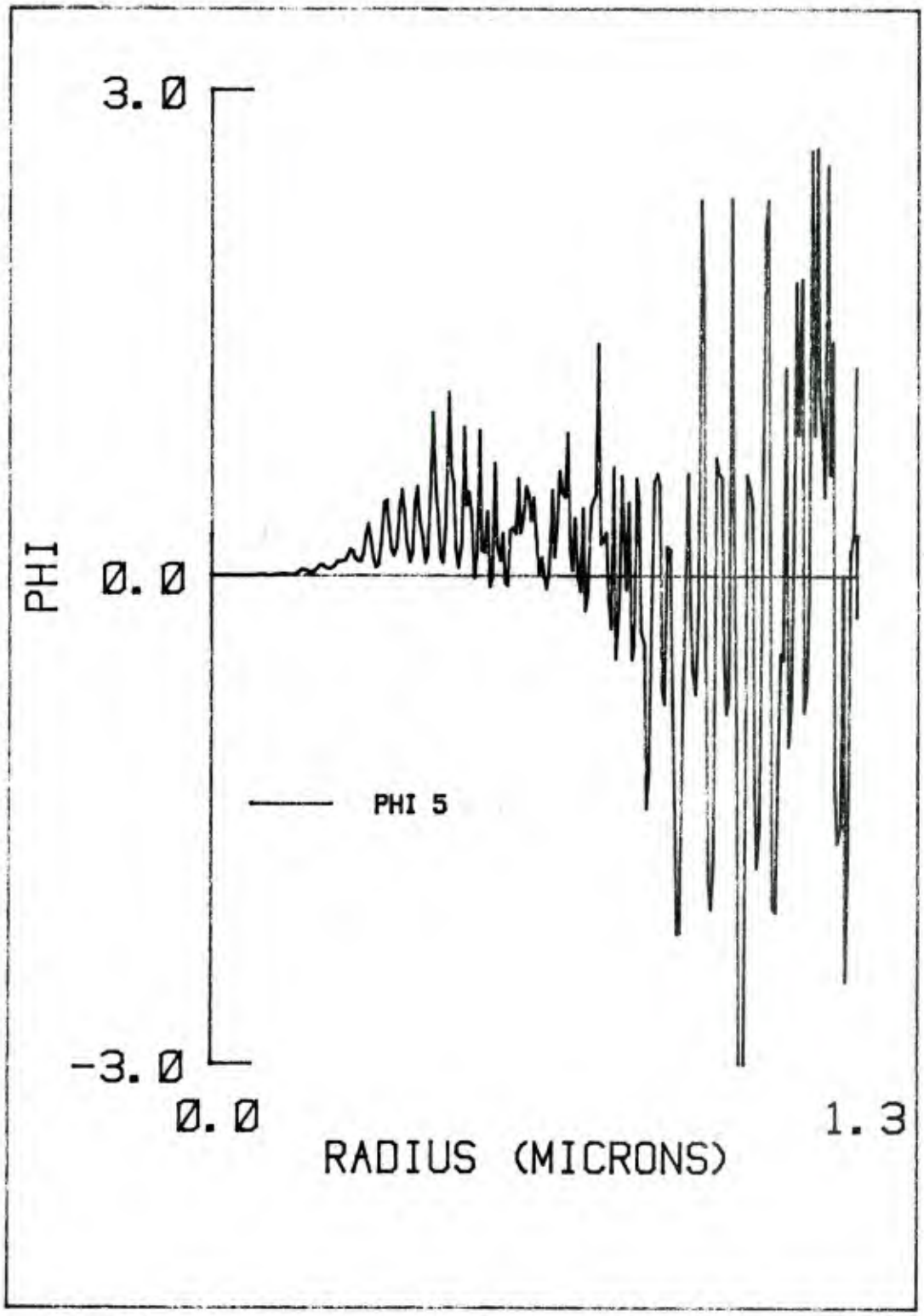

Figure B-15. The Ten Most Significant Eigenfunctions for the Baselien Case: ϕ_5

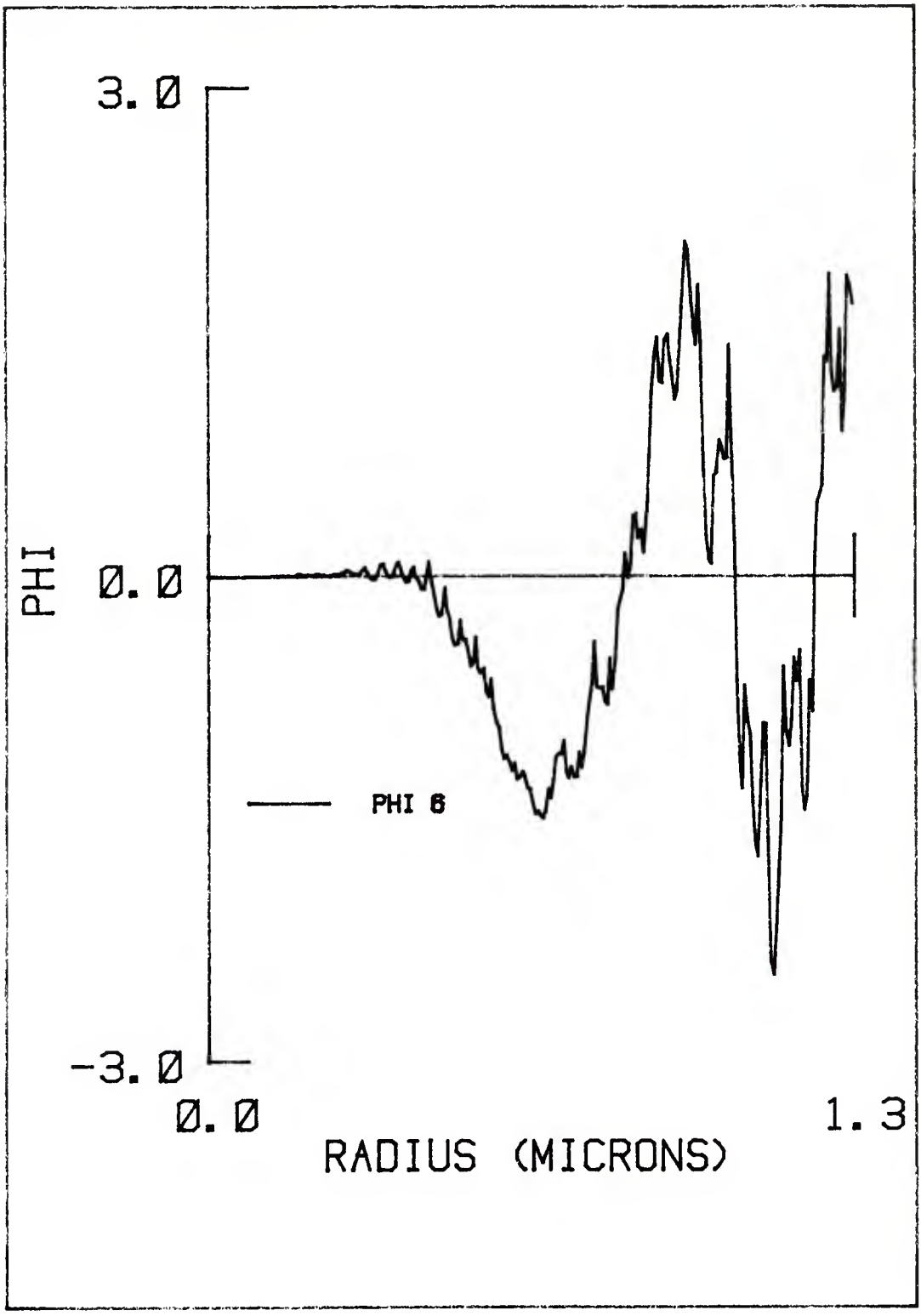

Figure B-16. The Ten most Significant Eigenfunctions for the Baseline Case: ϕ_6

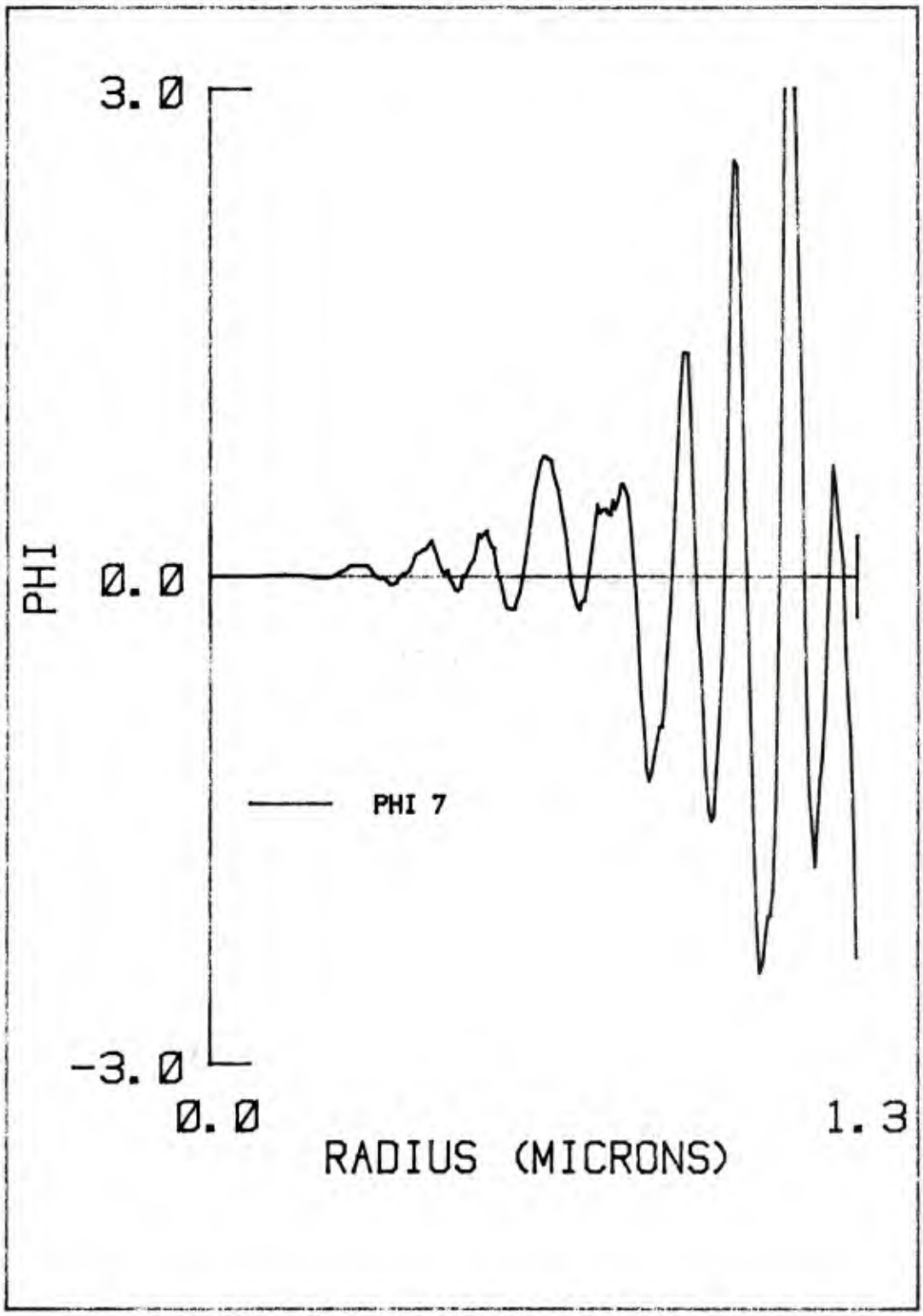

Figure B-17. The Ten Most Significant Eigenfunctions for the Baseline Case: ϕ_7

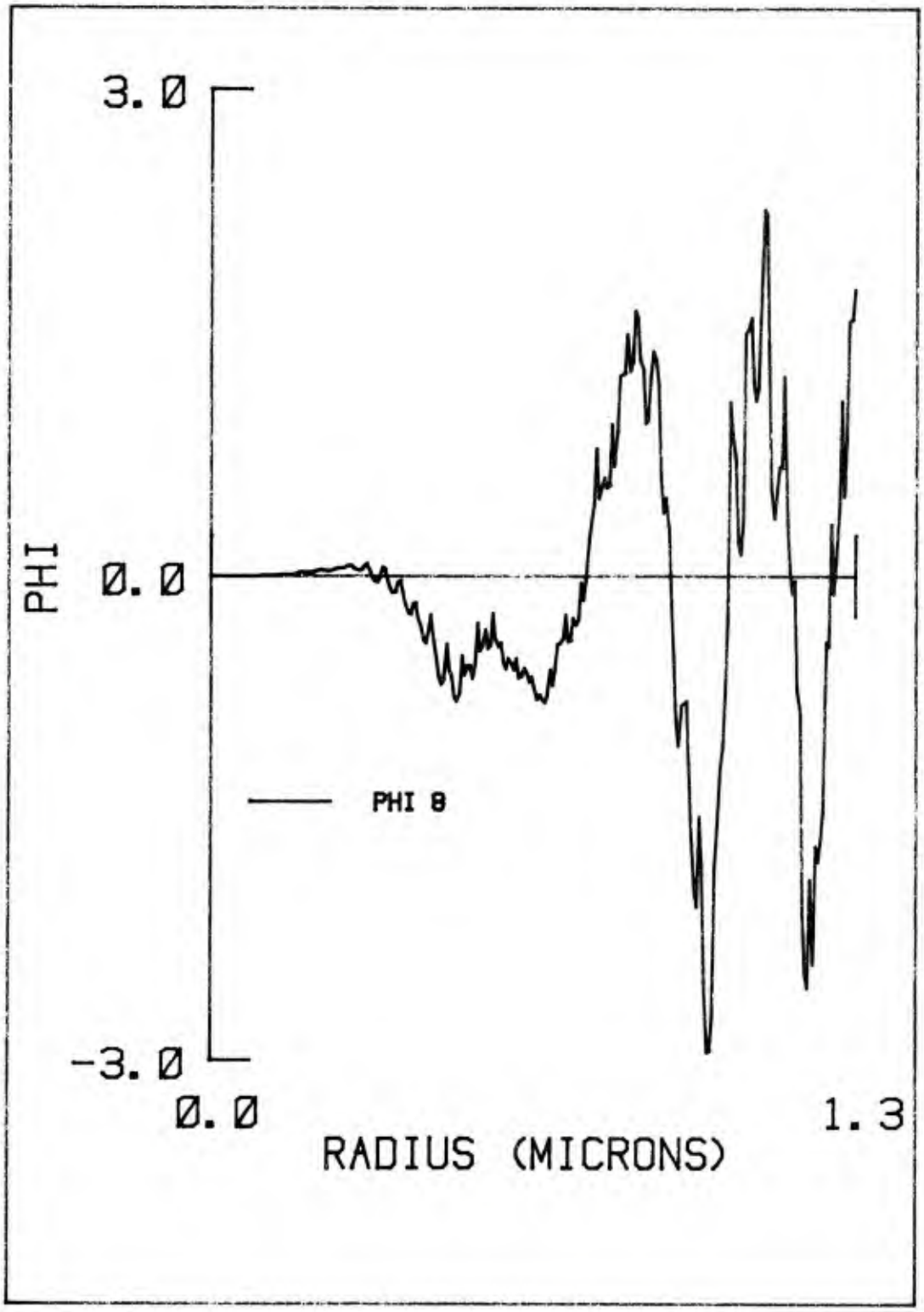

Figure B-18. The Ten Most Significant Eigenfunctions for the Baseline Case: ϕ_8

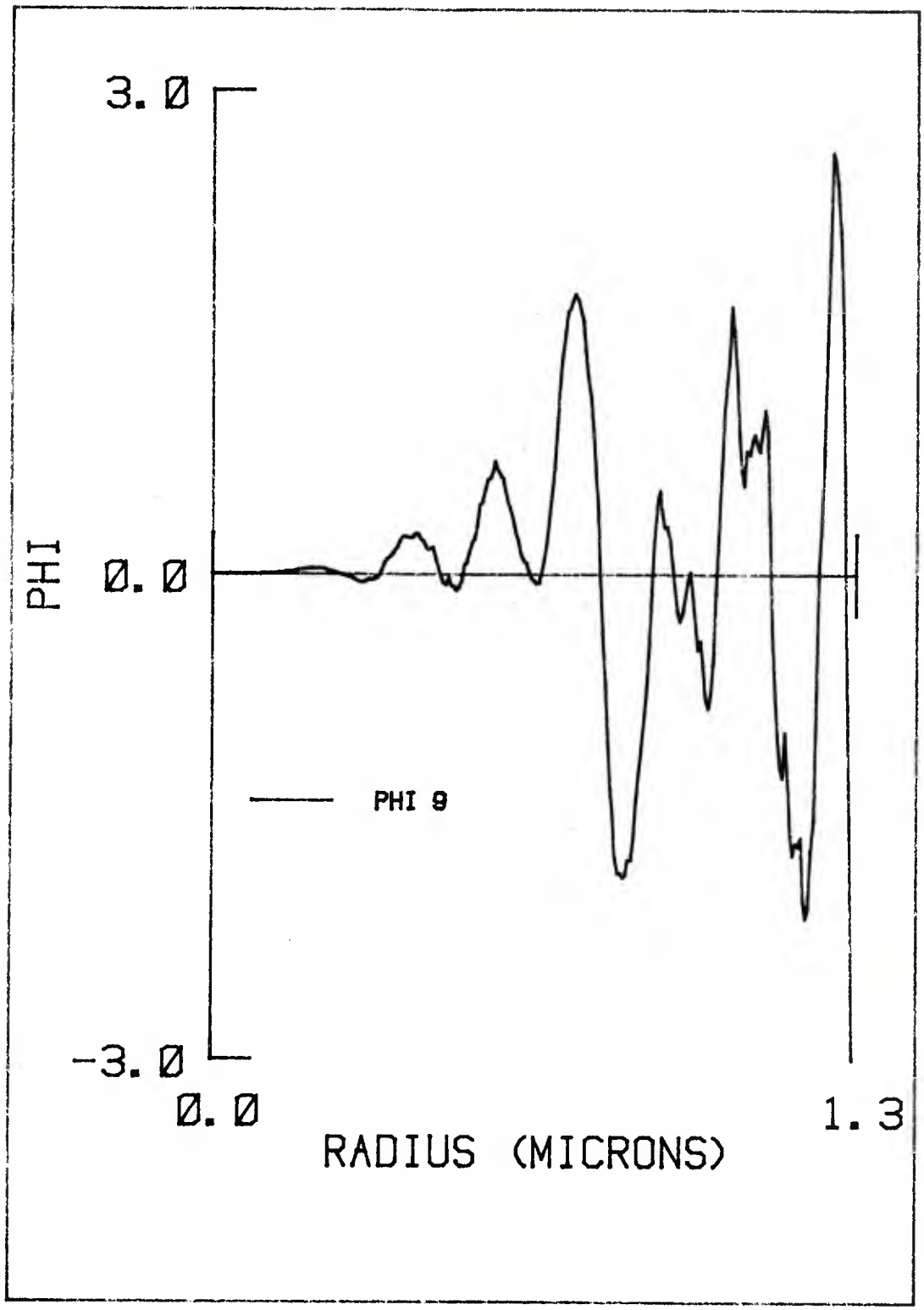

Figure B-19. The Ten Most Significant Eigenfunctions for the Baseline Case: ϕ_9

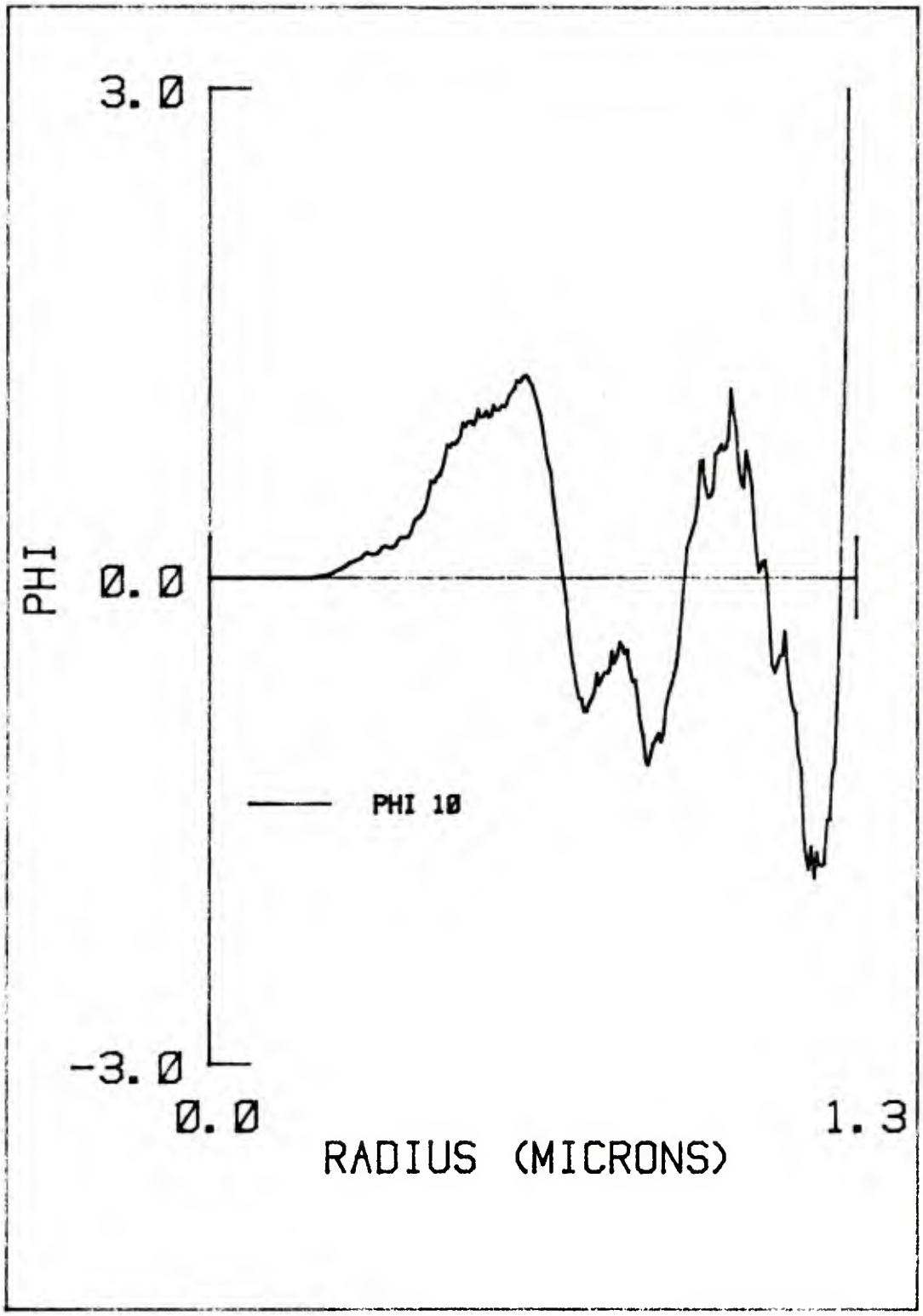

Figure B-20. The Ten Most Significant Eigenfunctions for the Baseline Case: ϕ_{10}

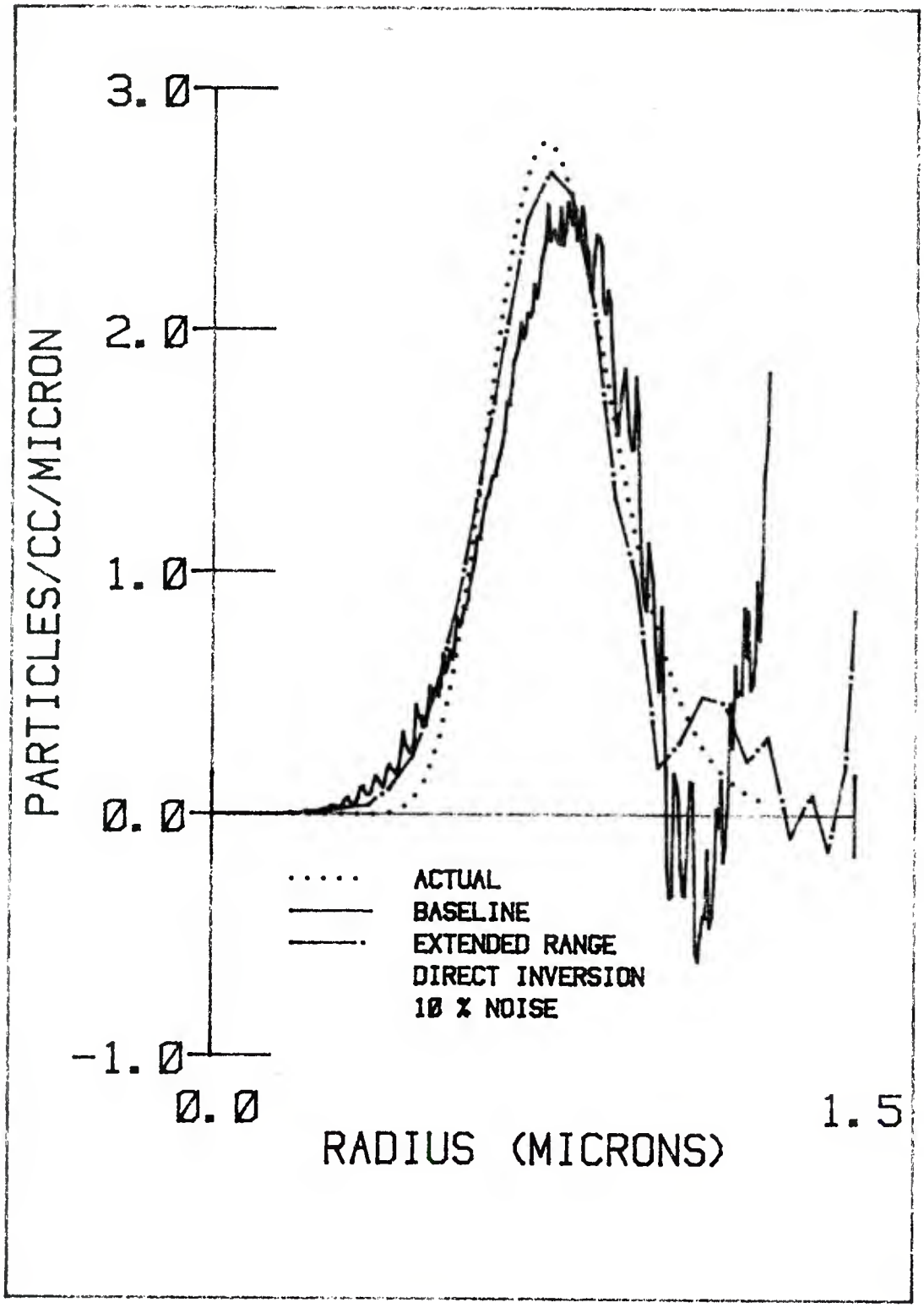

Figure B-21. Direct Inversion Sensitivity to Extended Radius Range: Baseline Twelve Measurements

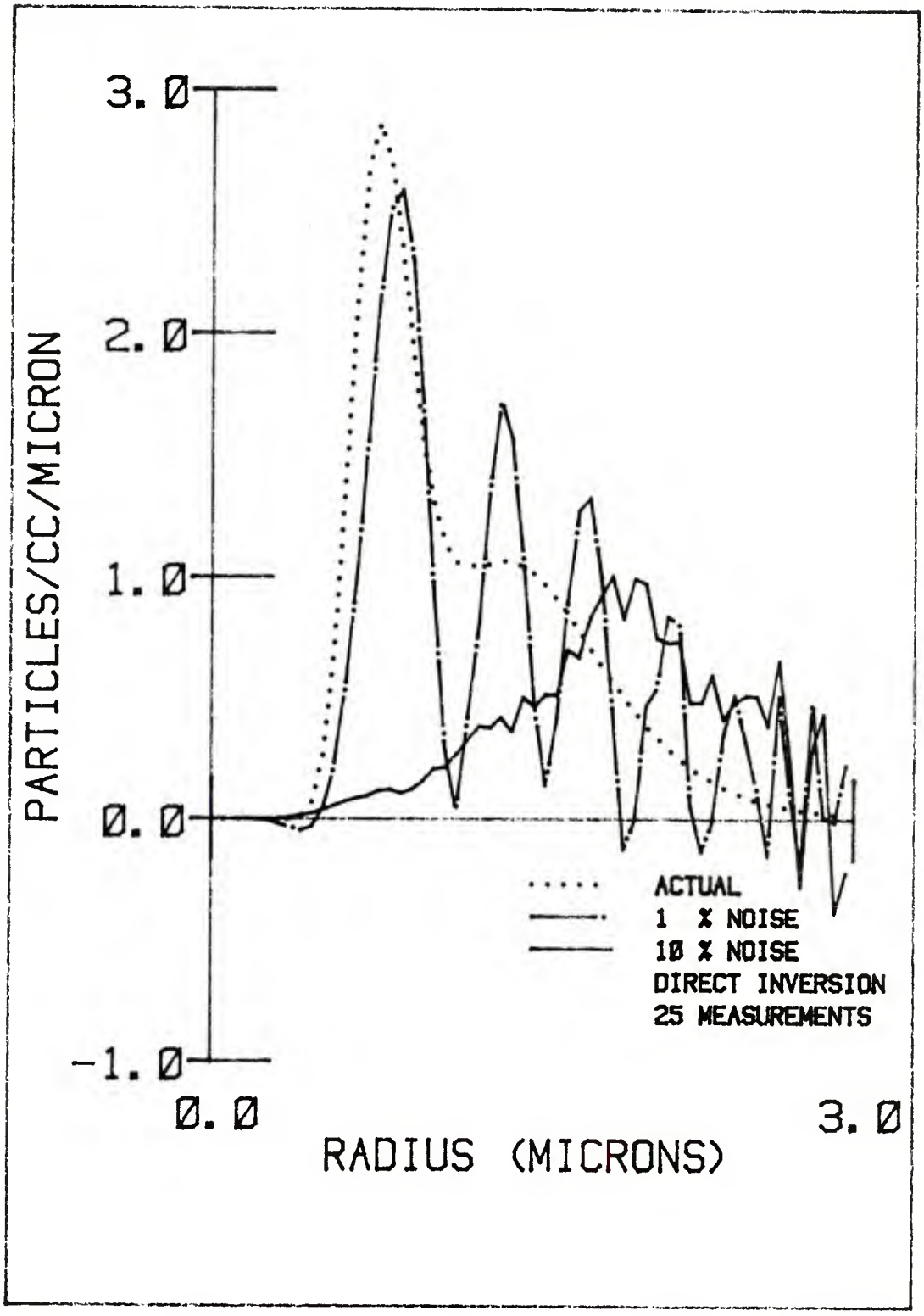

Figure B-22. Direct Inversion Sensitivity to Extended Range and Distribution: Bimodal

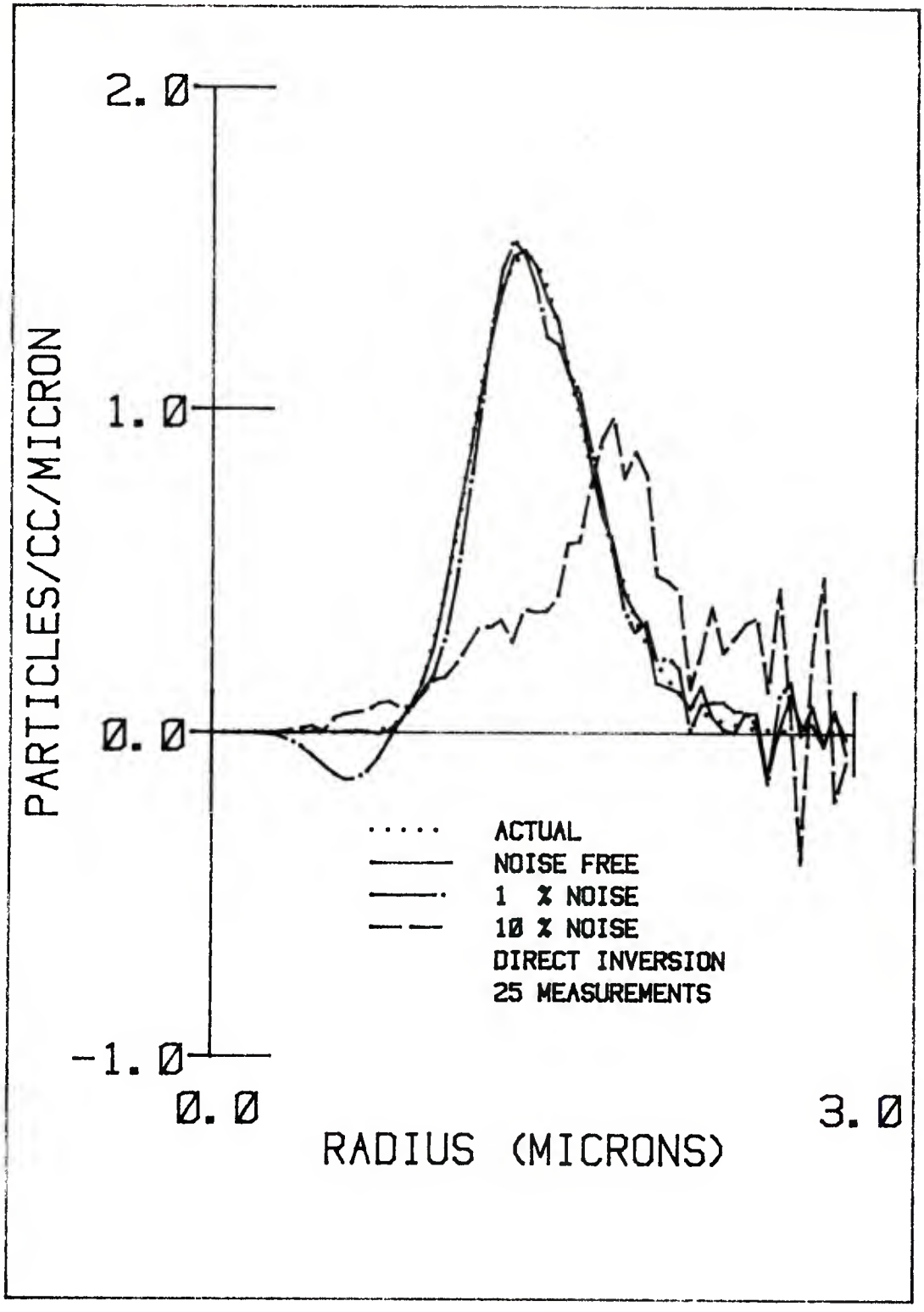

Figure B-23. Direct Inversion Sensitivity to Extended Range and Distribution: Increased Geometric Mean Diameter

DISTRIBUTION LIST FOR ARCSL-CR-82047

Names	Copies
CHEMICAL SYSTEMS LABORATORY	
ATTN: DRDAR-CLB	1
ATTN: DRDAR-CLB-C	1
ATTN: DRDAR-CLB-P	1
ATTN: DRDAR-CLB-PS	4
ATTN: DRDAR-CLB-R	1
ATTN: DRDAR-CLB-T	1
ATTN: DRDAR-CLB-TE	1
ATTN: DRDAR-CLC-B	1
ATTN: DRDAR-CLC-C	1
ATTN: DRDAR-CLF	1
ATTN: DRDAR-CLJ-R	2
ATTN: DRDAR-CLJ-L	2
ATTN: DRDAR-CLJ-M	1
ATTN: DRDAR-CLN	1
ATTN: DRDAR-CLN-S	1
ATTN: DRDAR-CLN-ST	1
ATTN: DRDAR-CLT	1
ATTN: DRDAR-CLY-A (Pennsyle, Hundley)	2
ATTN: DRDAR-CLY-R	1
COPIES FOR AUTHOR(S)	
Research Division (CPO)	25
RECORD COPY: DRDAR-CLB-A	1
DEPARTMENT OF DEFENSE	
Defense Technical Information Center	
ATTN: DTIC-DDA-2	2
Cameron Station, Building 5	
Alexandria, VA 22314	
Director	
Defense Intelligence Agency	
ATTN: DB-4G1	1
Washington, DC 20301	
Deputy Under Secretary of Defense for	
Research and Engineering (R&AT)	
ATTN: Dr. Musa	1
ATTN: COL Friday	1
ATTN: COL Winter	1
Washington, DC 20301	
Defense Advanced Research Projects Agency	
ATTN: Dr. Tegnelia	1
Washington, DC 20301	

Names	Copies
Advanced Research Projects Agency	1
1400 Wilson Boulevard	
Arlington, VA 22209	
DEPARTMENT OF THE ARMY	
HQDA	
ATTN: DAMO-NCC	1
ATTN: DAMO-NC/COL Robinson (P)	1
WASH DC 20310	
HQ DA	
Office of the Deputy Chief of Staff for	
Research, Development & Acquisition	
ATTN: DAMA-CSS-C	1
Washington, DC 20310	
HQ Sixth US Army	
ATTN: AFKC-OP-NBC	1
Presidio of San Francisco, CA 94129	
Commander	
DARCOM, STITEUR	
ATTN: DRXST-STI	1
Box 48, APO New York 09710	
Commander	
USASTCFEO	
ATTN: MAJ Mikeworth	1
APO San Francisco 96328	
Army Research Office	
ATTN: DRXRO-CB (Dr. R. Ghirardelli)	1
ATTN: DRXRO-GS	1
ATTN: Dr. W. A. Flood	1
P.O. Box 12211	
Research Triangle Park, NC 27709	
HQDA ODUSA (OR)	
ATTN: Dr. H. Fallin	1
Washington, DC 20310	
HQDA (DAMO-RQD)	
ATTN: MAJ C. Collat	1
Washington, DC 20310	

HQDA, OCE
ATTN: DAEN-RDM (Dr. Gomez) 1
Massachusetts Ave, NW
Washington, DC 20314

OFFICE OF THE SURGEON GENERAL

Commander
US Army Medical Research and
Development Command
ATTN: SGRD-UBG (Mr. Eaton) 1
ATTN: SGRD-UBG-OT (CPT Johnson) 1
ATTN: LTC Don Gensler 1
Fort Detrick, MD 21701

Commander
US Army Medical Bioengineering Research
and Development Laboratory
ATTN: SGRD-UBD-AL, Bldg 568 1
Fort Detrick, Frederick, MD 21701

Commander
USA Medical Research Institute of
Chemical Defense
ATTN: SGRD-UV-L 1
Aberdeen Proving Ground, MD 21010

US ARMY MATERIEL DEVELOPMENT AND
READINESS COMMAND

Commander
US Army Materiel Development and
Readiness Command
ATTN: DRCDE-DM 1
ATTN: DRCLDC 1
ATTN: DRCMT 1
ATTN: DRCSF-P 1
ATTN: DRCSF-S 1
ATTN: DRCDL (Mr. N. Klein) 1
ATTN: DRCBSI-EE (Mr. Giambalvo) 1
ATTN: DRCDMD-ST (Mr. T. Shirata) 1
5001 Eisenhower Ave
Alexandria, VA 22333

Commander
US Army Foreign Science & Technology Center
ATTN: DRXST-MT3 1
ATTN: DRXST-MT3 (Poleski) 1
220 Seventh St., NE
Charlottesville, VA 22901

Director
DARCOM Field Safety Activity
ATTN: DRXOS-SE (Mr. Yutmeyer) 1
Charlestown, IN 47111

PM Smoke/Obscurants
ATTN: DRCPM-SMK-E (A. Van de Wal) 1
ATTN: DRCPM-SMK-M 1
ATTN: DRCPM-SMK-T 1
Aberdeen Proving Ground, MD 21005

Director
US Army Materiel Systems Analysis Activity
ATTN: DRXSY-MP 1
ATTN: DRXSY-CA (Mr. Metz) 1
ATTN: DRXSY-FJ (J. O'Bryon) 1
ATTN: DRXSY-GP (Mr. Fred Campbell) 1
Aberdeen Proving Ground, MD 21005

USA AVIATION RESEARCH AND
DEVELOPMENT COMMAND

Director
Applied Technology Lab
USARTL (AVRADCOM)
ATTN: DAVDL-ATL-ASV 1
ATTN: DAVDL-ATL-ASW 1
ATTN: DAVDL-EV-MOS (Mr. Gilbert) 1
Ft. Eustis, VA 23604

Commander
USA Avionics R&D Activity
ATTN: DAVAA-E(M. E. Sonatag) 1
Ft. Monmouth, NJ 07703

USA MISSILE COMMAND

Commander
US Army Missile Command
Director, Energy Directorate
ATTN: DRSMI-RHFT 1
ATTN: DRSMI-RMST 1
ATTN: DRSMI-YLA (N. C. Katos) 1
Redstone Arsenal, AL 35809

Commander
US Army Missile Command
Redstone Scientific Information Center
ATTN: DRSHI-REO (Mr. Widenhofer) 1
ATTN: DRSMI-RGT (Mr. Matt Maddix) 1
ATTN: DRDMI-CGA (Dr. B. Fowler) 1
ATTN: DRDMI-KL (Dr. W. Wharton) 1
ATTN: DRDMI-TE (Mr. H. Anderson) 1
Redstone Arsenal, AL 35809

Commander
US Army Missile Command
Redstone Scientific Information Center
ATTN: DRSMI-RPR (Documents) 1
Redstone Arsenal, AL 35809

USA COMMUNICATIONS-ELECTRONICS COMMAND

Commander
USA Communications-Electronics Command
ATTN: DRSEL-WL-S (Mr. J. Charlton) 1
Ft. Monmouth, NJ 07703

Commander
USA Electronics Research and
Development Command
ATTN: DRDEL-CCM (Dr. J. Scales) 1
ATTN: DELHD-RT-CB (Dr. Sztankay) 1
Adelphi, MD 20783

Commander
Harry Diamond Laboratories
ATTN: DRXDO-RCB (Dr. Donald Wortman) 1
ATTN: DRXDO-RCB (Dr. Clyde Morrison) 1
ATTN: DRXDO-RDC (Mr. D. Giglio) 1
2800 Powder Mill Road
Adelphi, MD 20783

Commander
USA Materials & Mechanics Research Center
ATTN: DRXMR-KA (Dr. Saul Isserow) 1
Watertown, MA 02172

Commander
USA Cold Region Research Engineering Laboratory
ATTN: George Aitken 1
Hanover, NH 03755

Commander/Director
Combat Surveillance and Target
Acquisition Laboratory
ERADCOM
ATTN: DELCS-R (E. Frost) 1
Ft. Monmouth, NJ 07703

Director
Atmospheric Sciences Laboratory
ATTN: DELAS-AS (Dr. Charles Bruce) 1
ATTN: DELAS-AS-P (Mr. Tom Pries) 1
ATTN: DELAS-EO-EN (Dr. Donald Snider) 1
ATTN: DELAS-EO-EN (Mr. James Gillespie) 1
ATTN: DELAS-EO-ME (Dr. Frank Niles) 1
ATTN: DELAS-EO-ME (Dr. Ronald Pinnick) 1
ATTN: DELAS-EO-MO (Dr. Melvin Heaps) 1
ATTN: DELAS-EO-MO (Dr. R. Sutherland) 1
ATTN: DELAS-EO-S (Dr. Louis Duncan) 1
White Sands Missile Range, NM 88002

US ARMY ARMAMENT RESEARCH AND
DEVELOPMENT COMMAND

Commander
US Army Armament Research and
Development Command
ATTN: DRDAR-LCA-L 1
ATTN: DRDAR-LCE-C 1
ATTN: DRDAR-LCU-CE 1
ATTN: DRDAR-NC (COL Lymn) 3
ATTN: DRDAR-SCA-T 1
ATTN: DRDAR-SCF 1
ATTN: DRDAR-SCP 1
ATTN: DRDAR-SCS 1
ATTN: DRDAR-TDC (Dr. D. Gyorog) 1
ATTN: DRDAR-TSS 2
ATTN: DRCPM-CAWS-AM 1
Dover, NJ 07801

US Army Armament Research and
Development Command
ATTN: DRDAR-TSE-OA (Robert Thresher) 1
National Space Technology Laboratories
NSTL Station, MS 39529

Requirements and Analysis Office
Foreign Intelligence and Threat
Projection Division
ATTN: DRDAR-RAI-C 1
Aberdeen Proving Ground, MD 21010

Commander
ARRADCOM
ATTN: DRDAR-QAC-E 1
Aberdeen Proving Ground, MD 21010

Director
USA Ballistic Research Laboratory
ARRADCOM
ATTN: DRDAR-BLB 1
ATTN: DRDAR-TSB-S 1
Aberdeen Proving Ground, MD 21005

US ARMY ARMAMENT MATERIEL READINESS COMMAND

Commander
US Army Armament Materiel Readiness Command
ATTN: DRSAR-ASN 1
ATTN: DRSAR-IRI-A 1
ATTN: DRSAR-LEP-L 1
ATTN: DRSAR-SF 1
Rock Island, IL 61299

Commander
US Army Dugway Proving Ground
ATTN: Technical Library (Docu Sect) 1
Dugway, UT 84022

US ARMY TRAINING & DOCTRINE COMMAND

Commandant
US Army Infantry School
ATTN: CTDD, CSD, NBC Branch 1
Fort Benning, GA 31905

Commandant
US Army Missile & Munitions Center and School
ATTN: ATSK-CM 1
Redstone Arsenal, AL 35809

Commander
US Army Logistics Center
ATTN: ATCL-MG 1
Fort Lee, VA 23801

Commandant
US Army Chemical School
ATTN: ATZN-CM-C 1
ATTN: ATZN-CM-AD 2
ATTN: ATZN-CN-CDM (Dr. J. Scully) 1
Fort McClellan, AL 36205

Commander
USAAVNC
ATTN: ATZQ-D-MS 1
Fort Rucker, AL 36362

Commander
USA Combined Arms Center and Fort Leavenworth
ATTN: ATZL-CAM-IM 1
ATTN: ATZL-CA-SAN 1
ATTN: ATZL-CA-TM-K 1
Fort Leavenworth, KS 66027

Commander
US Army Infantry Center
ATTN: ATSH-CD-MS-C 1
ATTN: ATSH-CD-MS-F 1
ATTN: ATZB-DPT-PO-NBC 1
Fort Benning, GA 31905

Commander
USA Training and Doctrine Command
ATTN: ATCD-N 1
ATTN: ATCD-TEC (Dr. M. Pastel) 1
ATTN: ATCD-Z 1
Fort Monroe, VA 23651

Commander
US Army Armor Center
ATTN: ATZK-CD-MS 1
ATTN: ATZK-PPT-PO-C 1
Fort Knox, KY 40121

Commander
US Army TRADOC System Analysis Activity
ATTN: ATAA-SL 1
ATTN: ATAA-TDB (L. Dominguez) 1
White Sands Missile Range, NM 88002

Commander
USA Field Artillery School
ATTN: ATSF-GD-RA 1
Ft. Sill, OK 73503

Director
USA Concepts Analysis Agency
ATTN: MOCA-SMC (Hal Hock) 1
8120 Woodmont Avenue
Bethesda, MD 20014

Los Alamos National Laboratory
ATTN: T-DOT, MS B279 (S. Gerstl) 1
Los Alamos, NM 87545

US ARMY TEST & EVALUATION COMMAND

Commander
US Army Test & Evaluation Command
ATTN: DRSTE-CM-F 1
ATTN: DRSTE-CT-T 1
ATTN: DRSTE-AD-M (Warren Balty) 1
Aberdeen Proving Ground, MD 21005

Commander
USA EPG
ATTN: STEEP-MM-IS 1
ATTN: STEEP-MT-DS (CPT Decker) 1
Ft. Huachuca, AZ 85613

Commander
Dugway Proving Ground
ATTN: STEDP-MT (Dr. L. Solomon) 1
Dugway, UT 84022

DEPARTMENT OF THE NAVY

Commander
Naval Research Laboratory
ATTN: Code 5709 (Mr. W. E. Howell) 1
ATTN: Code 6532 (Mr. Curcio) 1
ATTN: Code 6532 (Mr. Trusty) 1
ATTN: Code 6530-2 (Mr. Gordon Stamm) 1
ATTN: Code 8320 (Dr. Lothar Ruhnke) 1
ATTN: Code 8326 (Dr. James Fitzgerald) 1
ATTN: Code 43202 (Dr. Hermann Gerber) 1
4555 Overlook Avenue, SW
Washington, DC 20375

Chief, Bureau of Medicine & Surgery
Department of the Navy
ATTN: MED 3C33 1
Washington, DC 20372

Commander
Naval Air Systems Command
ATTN: Code AIR-301C (Dr. H. Rosenwasser) 1
ATTN: Code AIR-5363 (D. C. Caldwell) 1
Washington, DC 20361

Commander
Naval Sea Systems Command
ATTN: SEA-62Y13 (LCDR Richard Gilbert) 1
ATTN: SEA-62Y21 (A. Kanterman) 1
ATTN: SEA-62Y21 (LCDR W. Major) 1
Washington, DC 20362

Project Manager
Theatre Nuclear Warfare Project Office
ATTN: TN-09C 1
Navy Department
Washington, DC 20360

Institute for Defense Analysis 1
400 Army-Navy Drive
Arlington, VA 22202

Commander
Naval Surface Weapons Center
Dahlgren Laboratory
ATTN: DX-21 1
ATTN: Mr. R. L. Hudson 1
ATTN: F-56 (Mr. Douglas Marker) 1
Dahlgren, VA 22448

Commander
Naval Intelligence Suport Center 1
ATTN: Code 434 (H. P. St.Aubin) 1
4301 Suitland Road
Suitland, MD 20390

Commander
Naval Explosive Ordnance Disposal
Technology Center
ATTN: AC-3 1
Indian Head, MD 20640

Officer-in-Charge
Marine Corps Detachment 1
Naval Explosive Ordnance Disposal
Technology Center
Indian Head, MD 20640

Commander
Naval Air Development Center
ATTN: Code 2012 (Dr. Robert Helmbold) 1
Warminster, PA 18974

Commander
Naval Weapons Center
ATTN: Code 382 (L. A. Mathews) 1
ATTN: Code 3882 (Dr. C. E. Dinerman) 1
ATTN: Code 3918 (Dr. Alex Shlanta) 1
China Lake, CA 93555

Commanding Officer
Naval Weapons Support Center
Applied Sciences Department
ATTN: Code 50C, Bldg 190 1
ATTN: Code 502 (Carl Lohkamp) 1
Crane, IN 47522

US MARINE CORPS

Commanding General
Marine Corps Development and
Education Command
ATTN: Fire Power Division, D091 1
Quantico, VA 22134

DEPARTMENT OF THE AIR FORCE

HQ AFLC/LOWMM 1
Wright-Patterson AFB, OH 45433

HQ AFSC/SDZ 1
ATTN: CPT D. Riediger
Andrews AFB, MD 20334

USAF TAWC/THL 1
Eglin AFB, FL 32542

USAF SC
ATTN: AD/YQ (Dr. A. Vasiloff) 1
ATTN: AD/YQO (MAJ Owens) 1
Eglin AFB, FL 32542

AFAMRL/TS
ATTN: COL Johnson 1
Wright-Patterson AFB, OH 45433

Commander
Hanscom Air Force Base
ATTN: AFGL-POA (Dr. Frederick Volz) 1
Bedford, MA 01731

Headquarters
Tactical Air Command
ATTN: DRP 1
Langley AFB, VA 23665

AFOSR/NE
ATTN: MAJ H. Winsor 1
Bolling AFB, DC 20332

AD/SRO 1
Eglin AFB, FL 32542

Dr. Charles Arpke 1
OSV Field Office
P.O. Box 1925
Eglin AFB, FL 32542

OUTSIDE AGENCIES

Battelle, Columbus Laboratories
ATTN: TACTEC 1
505 King Avenue
Columbus, OH 43201

Toxicology Information Center, JH 652
National Research Council 1
2101 Constitution Ave., NW
Washington, DC 20418

Dr. W. Michael Farmer, Assoc Prof, Physics
University of tennessee Space Institute 1
Tullahoma, TN 37388

ADDITIONAL ADDRESSEES

Office of Missile Electronic Warfare
ATTN: DELEW-M-T-AC (Ms Arthur) 1
White Sands Missile Range, NM 88002

US Army Mobility Equipment Research and
Development Center
ATTN: DROME-RT (Mr. O. F. Kezer) 1
Fort Belvoir, VA 22060

Director
US Night Vision and EO Laboratories
ATTN: DRSEL-NV-VI (Dr. R. G. Buser) 1
ATTN: DRSEL-NV-VI (Mr. R. Bergemann) 1
ATTN: DELNV-VI (Luanne Obert) 1
ATTN: DELNV-L (D. N. Spector) 1
Fort Belvoir, VA 23651

Commandant
Academy of Health Sciences, US Army
ATTN: HSHA-CDH 1
ATTN: HSHA-IPM 2
Fort Sam Houston, TX 78234

Commander
US Army Armament Research and
Development Command
ATTN: DRDAR-LCE (Mr. Scott Morrow) 1
Dover, NJ 07801